

Curved factor analysis with the Ellipsoid-Gaussian distribution

Hanyu Song David B. Dunson

Department of Statistical Science
Duke University

January 24, 2022

Abstract

There is a need for new models for characterizing dependence in multivariate data. The multivariate Gaussian distribution is routinely used, but cannot characterize nonlinear relationships in the data. Most non-linear extensions tend to be highly complex; for example, involving estimation of a non-linear regression model in latent variables. In this article, we propose a relatively simple class of Ellipsoid-Gaussian multivariate distributions, which are derived by using a Gaussian linear factor model involving latent variables having a von Mises-Fisher distribution on a unit hyper-sphere. We show that the Ellipsoid-Gaussian distribution can flexibly model curved relationships among variables with lower-dimensional structures. Taking a Bayesian approach, we propose a hybrid of gradient-based geodesic Monte Carlo and adaptive Metropolis for posterior sampling. We derive basic properties and illustrate the utility of the Ellipsoid-Gaussian distribution on a variety of simulated and real data applications.

Key words: Dimensionality reduction; Ellipse; Latent factors; PCA; Sphere; von Mises-Fisher distribution

1 Introduction

The multivariate Gaussian distribution is routinely used, relying on a rich collection of methods for inference on the covariance structure. Factor analysis is particularly popular, due to its combination of simplicity and flexibility. The generic form of a Gaussian linear factor model is

$$x_i = c + \Lambda \eta_i + \epsilon_i, \quad \epsilon_i \sim N_p(0, \Sigma), \quad (i = 1, \dots, n), \quad (1)$$

where x_i is p -dimensional, Λ is a $p \times k$ factor loadings matrix, $\eta_i \sim N_k(0, I_k)$ are latent factors and ϵ_i is an idiosyncratic error with covariance $\Sigma = \text{diag}(\sigma_1^2, \dots, \sigma_p^2)$. Conditional on the factors, the elements of x_i are independent; dependence is induced by marginalizing out the latent factors to obtain $x_i \sim N_p(c, \Omega)$ with $\Omega = \Lambda \Lambda^T + \Sigma$.

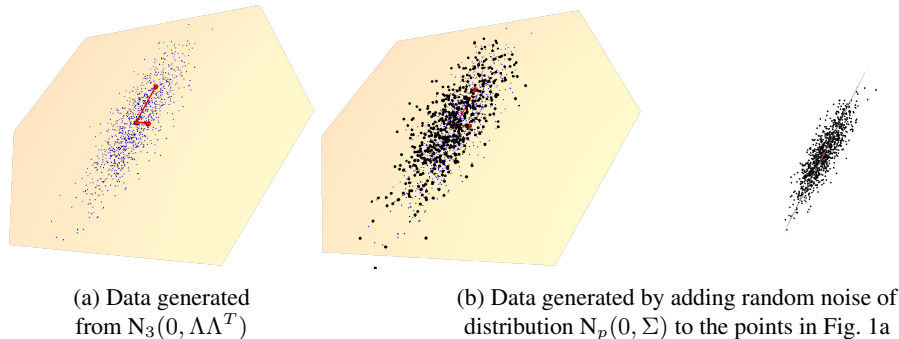


Figure 1: Demonstration of the Gaussian linear factor model with $p = 3, k = 2$. The yellow plane represents the column space of Λ and contains all of the blue points sampled from $N_3(0, \Lambda\Lambda^T)$. The red vectors represent eigenvectors of $\Lambda\Lambda^T$; equivalently the left singular vectors of Λ . The figure on the right shows the view perpendicular to the plane, illustrating that the data have a Gaussian distribution centered around the plane.

In genomics, for instance, x_i can be a massive vector of gene expression values; with genes within common pathways tending to co-express, it is natural to regard η_i as pathway characterizing factors (Carvalho et al., 2008). In practice, one typically chooses $k \ll p$. It is reasonable to suppose that the loadings matrix contains many zero entries, so that any single factor only impacts a relatively small number of elements of x_i . Hence, dimension reduction is often carried out through low rank and sparsity assumptions on the loadings matrix. See, for instance, Bhattacharya and Dunson (2011), Ghosh and Dunson (2009), and West (2003) and Z. Ma (2013).

Our work begins from the observation that the multivariate Gaussian distribution cannot characterize nonlinear relationships in data. Consider the Gaussian linear factor model. To generate data from $x_i \sim N_p(0, \Lambda\Lambda^T + \Sigma)$, we can first generate data from $N_p(0, \Lambda\Lambda^T)$ and then add random $N_p(0, \Sigma)$ noise. Figure 1 shows a simulation example with $p = 3, k = 2$. Figure 1a shows data simulated from $N_3(0, \Lambda\Lambda^T)$; since Λ has rank 2, this is a degenerate Gaussian distribution on a linear subspace spanned by the columns of Λ . After adding Gaussian noise with covariance Σ to the data in the plane, we obtain a distribution in \mathbb{R}^3 , as shown in Fig. 1b. The Gaussian linear factor model assumes that the data are centered around a linear space spanned by the columns of Λ , and therefore cannot capture curvature.

However, curved relationships are commonplace in real data. We provide two motivating examples; one is a speed flow data set on a California freeway (Einbeck & Dwyer, 2011) and the other is an ecological data set of horse mussels in New Zealand (Camden, 1989). Figure 2a shows that vehicle flow, per 5 minutes, and speed, in miles per hour, on the freeway have a curved relationship. Figure 2b shows that body measurements, such as edible muscle mass (M) and shell width (W), of the horse mussels have curved dependence.

There is a rich literature on nonlinear factor models that can capture curved dependence by replacing the linear loadings on η_i with a more complex mapping. A general model is given by $x_i = g(\eta_i) + \epsilon_i$, with the same assumptions as a Gaussian linear factor model but a nonlinear function g mapping $\mathbb{R}^k \rightarrow \mathbb{R}^p$. Popular nonparametric approaches include Gaussian process

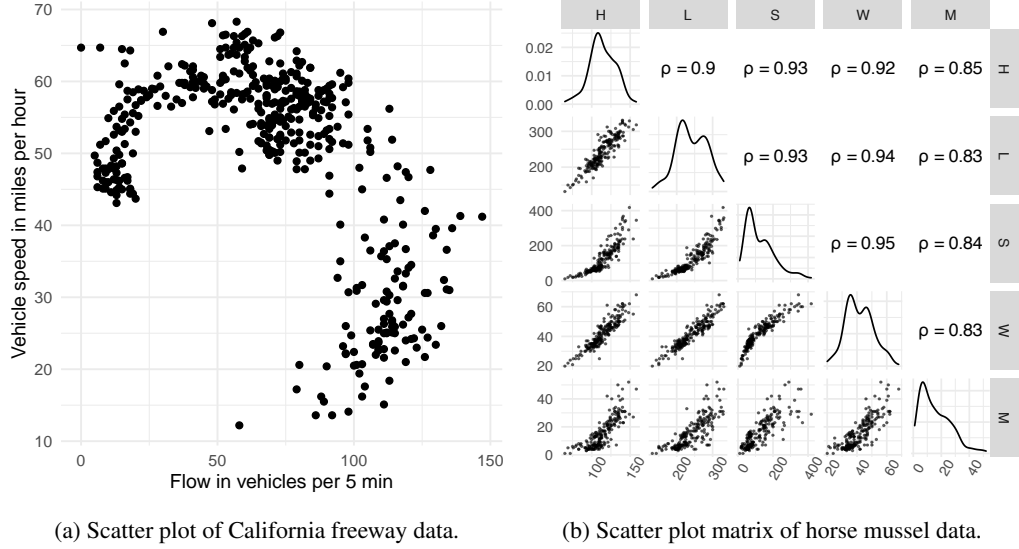


Figure 2: Scatter plots of two curved data sets. In particular, H, L, S, W, and M represent shell height (mm), shell length (mm), shell mass (g), shell width (mm) and muscle mass (g) respectively.

latent variables models, which give $g(\cdot)$ a Gaussian process prior (Li & Chen, 2016; Titsias & Lawrence, 2010), and variational auto encoders, which model $g(\cdot)$ using a deep neural network (Kingma & Welling, 2014; Rezende et al., 2014). Such methods are highly flexible but tend to be complex black boxes that have issues with reproducibility of results and non-identifiability, while being opaque to interpret.

An alternative is to mix Gaussian linear factor models to capture nonlinear structure in the data by local linear Gaussian models; for example, refer to the rich literature on mixtures of factor analyzers (Ghahramani & Hinton, 1997; McLachlan et al., 2003; Murphy et al., 2020). However, in defining a factor model for every component of a mixture model, such models are heavily parameterized and can be difficult to fit reliably and interpret. If there are not distinct clusters in the data but data have curved support, data will be broken up into many small clusters.

Other attempts to develop flexible parametric families of multivariate distributions have focused on capturing skewness and heavy tails in the data, among which the generalization of skew-elliptical distributions (Azzalini & Capitanio, 1999; Branco & Dey, 2001) constitutes a prominent subset. Starting with multivariate skew-normal distributions (Azzalini & Valle, 1996), there are extensions to multivariate skew- t (Arevalillo & Navarro, 2015; Gupta, 2003; Kim & Mallick, 2003), scale mixtures of skew-normal (Capitanio, 2020; Kim, 2008), skew-symmetric (Jupp et al., 2016) and even broader families (Azzalini & Capitanio, 2003; Genton & Loperfido, 2005; Landsman et al., 2017). An alternative extension of the skew-normal is the multivariate skew-slash distribution (Wang & Genton, 2006). Certain of the above distributions can induce curvature, but in an indirect and hard to interpret manner.

Hence, there is a need to develop simple parametric models to characterize nonlinear dependence

in data. In this article, we propose a class of parametric factor models that induce multivariate distributions supported near the surface of a hyper-ellipsoid. This Ellipsoid-Gaussian class is induced by using a Gaussian linear factor model with latent variables following a von Mises-Fisher distribution on a unit hyper-sphere. We show that the Ellipsoid-Gaussian distribution is surprisingly flexible in allowing curved relationships among variables and modeling of lower-dimensional structure, while including the Gaussian linear factor model as a special case. All proofs are in the Appendices.

2 The von Mises-Fisher linear factor model

To induce curved relationships among x_{i1}, \dots, x_{ip} , a starting point is distributions on a sphere. Let \mathcal{S}^{k-1} be a unit sphere in \mathbb{R}^k centered at the origin and \mathcal{S}^{k-1} be the probability measure of the uniform distribution on \mathcal{S}^{k-1} . A simple density with respect to \mathcal{S}^{k-1} for a random vector $z \in \mathcal{S}^{k-1}$ is $f(z; \mu, \tau) = C_k(\tau) \exp(\tau \mu^T z)$, where μ is the mean direction with $\|\mu\| = 1$, $\tau \geq 0$ is a concentration parameter, $C_k(\tau) = (\tau/2)^{k/2-1} \{\Gamma(k/2) I_{k/2-1}(\tau)\}^{-1}$ is the normalizing constant, and $I_v(\tau)$ denotes the modified Bessel function of the first kind of order v . This von Mises-Fisher density is symmetric about the mean direction μ , with τ controlling concentration—a larger τ corresponds to higher concentration around μ . The inner product between two unit vectors $\mu^T z$ parametrizes the cosine distance between μ and z . This metric has been used in high-dimensional directional data clustering, such as for text and gene-expression data (Banerjee et al., 2005; Gopal & Yang, 2014; Reisinger et al., 2010).

While the von Mises-Fisher distribution is not directly useful for the data x_i , since these data are not exactly on a sphere, it can be used for latent factors in model (1) as follows:

$$x_i = c + \Lambda \eta_i + \epsilon_i, \quad \epsilon_i \sim N_p(0, \Sigma), \quad \eta_i \sim \text{vMF}(\mu, \tau), \quad i = 1, \dots, n. \quad (2)$$

To better understand this model, we first define some notation. Let the singular value decomposition of Λ be $U_{p \times k} S_{k \times k} V_{k \times k}^T$, where $U^T U = I$, $V^T V = I$ and $S_{k \times k} = \text{diag}(s_1, \dots, s_k)$. The image of a unit sphere \mathcal{S}^{k-1} under the affine transformation $c + \Lambda \mathcal{S}^{k-1}$ is a k -dimensional ellipsoid in \mathbb{R}^p ; when $k < p$, the ellipsoid is degenerate. The center of the ellipsoid is c , its principal axes are represented by the left singular vectors U , and its semi-axes lengths by the singular values S . The image of \mathcal{S}^{k-1} after multiplication by Λ can be understood as sequentially transforming the sphere by each matrix in the factorization: since the sphere is rotationally invariant, the image \mathcal{S}^{k-1} under the rotation V^T is still itself; S stretches the sphere \mathcal{S}^{k-1} into an ellipsoid centered at the origin with principal axes parallel to the coordinate axes and semi-axes lengths equal to the singular values s_k ; finally, U rotates the ellipsoid such that the principal axes are parallel to the column vectors of U and embeds it into a k -dimensional linear subspace of \mathbb{R}^p . Adding c translates the ellipsoid such that its center becomes c . We then add Gaussian noise.

To visualize data generated from this model, consider an example with $p = 3, k = 2$. If we generate noiseless data from the model with $c = 0$, the points will lie on an ellipse as shown in Fig. 3a, with the center of the ellipse at the origin and the shape of the ellipse determined by Λ . The red line segments represent the principal axes of the ellipsoid and are also the left singular vectors of Λ . We then add Gaussian noise around the points in Fig. 3a to obtain the desired distribution, as visualized in Fig. 3b, where the points are distributed around a curved surface, the ellipsoid, and this is how the curvature is captured in the model.

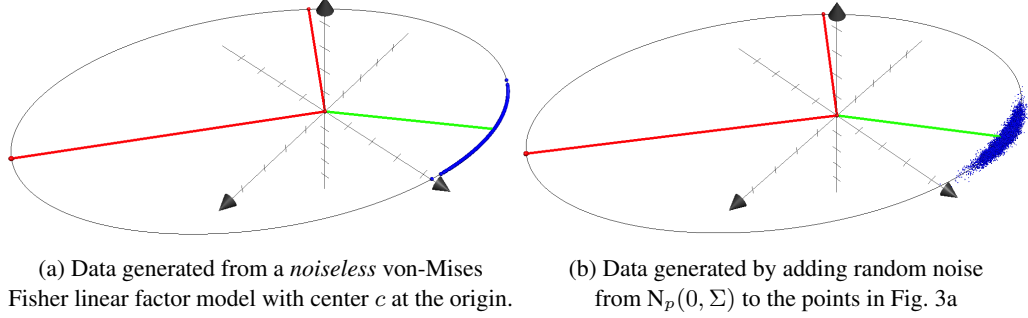


Figure 3: Demonstration of the von Mises-Fisher linear factor model with $p = 3, k = 2$. The green and red lines represent the mean direction $\Lambda\mu$ and principal axes of the ellipse, respectively.

Figure 4 shows more simulated examples from this model. The various shapes of the data clouds suggest tremendous flexibility of the model in accommodating different data — data that exhibit symmetry, asymmetry, uneven curvature or data that are close to Gaussian.

3 Ellipsoid-Gaussian distribution

Analogous to the Gaussian latent factor model, we wish to marginalize over the distribution of the latent factor η to obtain the marginal distribution of x ; we call the resulting distribution *Ellipsoid-Gaussian*. The density of x can be calculated in closed-form, and x is supported on the entirety of \mathbb{R}^p . In order to state the density, we recall the Fisher-Bingham distribution, which is a distribution on \mathcal{S}^{k-1} that includes the von Mises-Fisher distribution as a special case. A random vector y with a Fisher-Bingham distribution has density with respect to \mathcal{S}^{k-1} :

$$f(y; \kappa, \vartheta, A) = \frac{1}{\varsigma(\kappa\vartheta, A)} \exp(\kappa\vartheta^T y - y^T A y),$$

where $y, \vartheta \in \mathcal{S}^{k-1}$, $\kappa \geq 0$, $A \in \mathbb{R}^{p \times p}$ is a symmetric matrix, and $\varsigma(\kappa\vartheta, A)$ is a normalizing constant that is commonly estimated via a saddlepoint approximation (Kume & Wood, 2005) which is accurate, fast and numerically stable. The Fisher-Bingham distribution has been studied in Hoff (2009), J. T. Kent et al. (2013), and Wood (1988) and many other works.

Proposition 1 shows the marginal density of the Ellipsoid-Gaussian distribution.

Proposition 1. Assume $x = c + \Lambda\eta + \epsilon$, $\epsilon \sim N_p(0, \Sigma)$, $\eta \sim vMF(\mu, \tau)$, and $\Sigma = \text{diag}(\sigma_1^2, \dots, \sigma_p^2)$.

1. Marginalizing over the distribution of η yields density

$$f_{EG}(x) = \frac{C_k(\tau)}{(2\pi)^{\frac{p}{2}} \prod_{i=1}^p \sigma_i} \exp \left\{ -\frac{1}{2} (x - c)^T \Sigma^{-1} (x - c) \right\} \varsigma \left\{ \tau\mu + \Lambda^T \Sigma^{-1} (x - c), \frac{\Lambda^T \Sigma^{-1} \Lambda}{2} \right\},$$

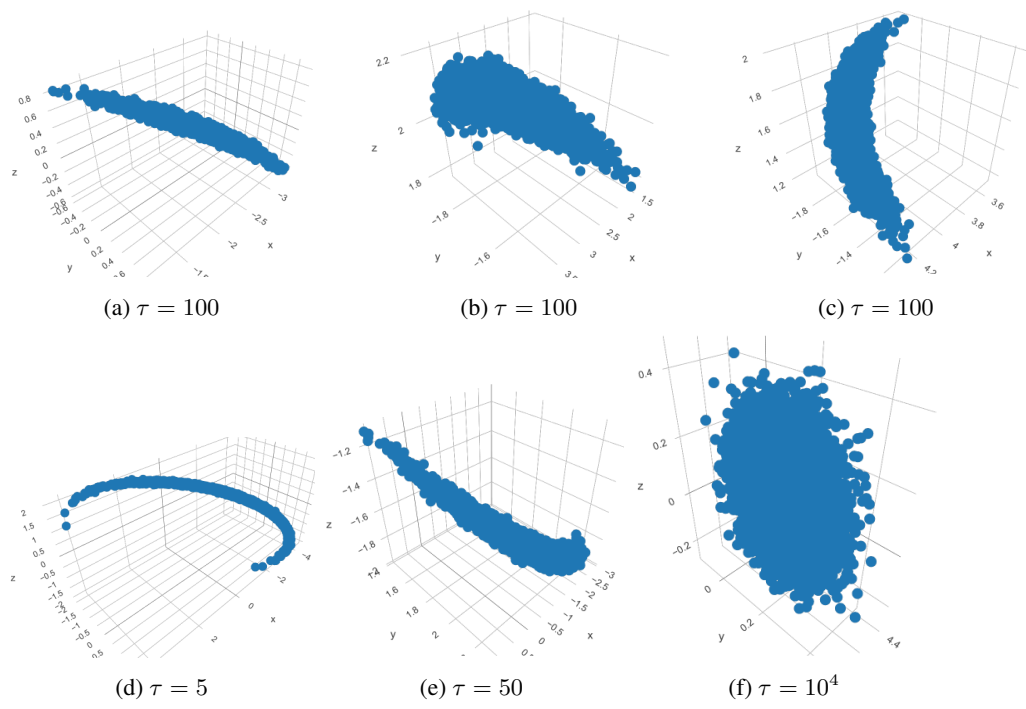


Figure 4: Scatter plots of data sampled from the Ellipsoid-Gaussian in \mathbb{R}^3 with varying parameters.

with respect to the Lebesgue measure on \mathbb{R}^p , where $\varsigma(\kappa\vartheta, A)$ is the normalizing constant in a Fisher-Bingham density.

2. The Fisher-Gaussian distribution (Mukhopadhyay et al., 2020) is a special case of the Ellipsoid-Gaussian distribution with $\Lambda = rI_p$ and $\Sigma = \sigma^2 I_p$.
3. The marginal distribution of any sub-vector of x also follows an Ellipsoid-Gaussian distribution. Specifically, suppose the index set of the random vector is $I \subset [p]$ and let subscript I represent elements from the rows of a matrix or elements from a vector, whose index is in set I . Then x_I follows a Ellipsoid-Gaussian with density

$$f_{EG}(x_I) = \frac{C_k(\tau)}{(2\pi)^{\frac{|I|}{2}} \prod_{i \in I} \sigma_i} \exp \left\{ -\frac{1}{2} (x_I - c_I)^T \Sigma_I^{-1} (x_I - c_I) \right\} \\ \varsigma \left\{ \tau\mu + \Lambda_I^T \Sigma_I^{-1} (x_I - c_I), \frac{\Lambda_I^T \Sigma_I^{-1} \Lambda_I}{2} \right\},$$

where $\Sigma_I = \text{diag}(\sigma_j, j \in I)$.

4. The expectation of x is $c + \rho_k(\tau)\Lambda\mu$, where $\rho_k(\tau) = I_{k/2}(\tau)/I_{k/2-1}(\tau)$.
5. The covariance of x is $\rho_k(\tau)/\tau\Lambda\Lambda^T + \{1 - \frac{k}{\tau}\rho_k(\tau) - \rho_k^2(\tau)\}\Lambda\mu(\Lambda\mu)^T + \Sigma$.

This Proposition has several interesting ramifications. The term ς is not part of the normalising constant as it depends on the random variable x ; this leads to some challenges in model fitting. The Fisher-Gaussian distribution in Mukhopadhyay et al., 2020 is a special case, which corresponds to the Ellipsoid-Gaussian with no dimension reduction ($p = k$), spherical Gaussian noise, and Λ being a scalar multiple of the identity matrix. In addition, unlike the Gaussian linear factor model, c is no longer the expectation of x , suggesting that we cannot simply center the data prior to analysis and remove c .

3.1 Identifiability of the model parameters

An Ellipsoid-Gaussian distribution contains parameters $\{c, \Lambda, \mu, \tau, \Sigma\}$ of total dimension $(p + 1)(k + 1) + p$. In this section, we show that some of these parameters are not identifiable.

Proposition 2. *In model (2), Λ is only identifiable up to orthogonal transformation.*

Figure 5 gives a visual representation of this proposition, which shows that the nonidentifiability of Λ is due to a transformation property of the von Mises-Fisher distribution. Model (1) shares this property, due to rotational invariance of the distribution of the latent factors $N(0, I_k)$, with the image of η under an orthogonal transformation Γ still being $N(0, I_k)$. In (2), however, an orthogonal transformation Γ of η results in a different von Mises-Fisher distribution, having the same concentration parameter τ but with a different mean vector $\Gamma\mu$. Therefore, a rotation of η necessarily results in a rotation in Λ as well. The following proposition provides further insights.

Proposition 3. *The moment generating function of the Ellipsoid-Gaussian distribution is*

$$M_{EG}(t) = \exp \left(t^T c + \frac{1}{2} t^T \Sigma t \right) \frac{C_k(\tau)}{C_k(\|\Lambda^T t + \tau\mu\|)}.$$

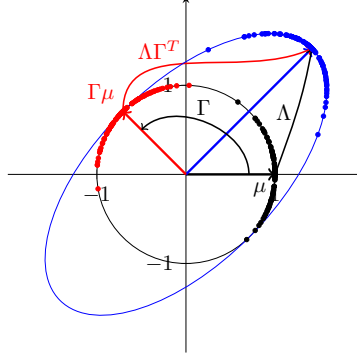


Figure 5: Rotating the samples from a $\text{vMF}(\mu, \tau)$ (black) by Γ results in samples from a $\text{vMF}(\Gamma\mu, \tau)$ (red). Mapping the black points by Λ and the red points by $\Lambda\Gamma^T$, respectively, results in the same set of points (blue).

This proposition suggests a different parameterization. Let

$$\|\Lambda^T t + \tau\mu\| = \sqrt{t^T \Lambda \Lambda^T t + 2\tau \Lambda\mu + \tau^2}.$$

Hence, the moment generating function depends on Λ and μ only through $\Lambda\Lambda^T$ and $\Lambda\mu$. By Proposition 1, $\Lambda\mu$ is the mean direction if the underlying ellipsoid is centered at the origin. The symmetric matrix $\Lambda\Lambda^T$ with spectral decomposition US^2U^T defines a k -dimensional ellipsoid consisting of points satisfying $x^T US^{-2}U^T x = 1$. Instead of using Λ and μ , we can view the distribution as being parameterized by the supporting ellipsoid and the mean direction $\Lambda\mu$.

The Ellipsoid-Gaussian distribution has mass centered around a hyper-ellipsoid, but real data are often concentrated on a small portion of the hyper-ellipsoid. Hence, there can be multiple sets of parameters corresponding to different hyper-ellipsoids that match the curvature of the data equally well. For example, to obtain a different fit to the points in Fig. 3b, we can move the center of an ellipsoid farther from the data cloud, while increasing the axis lengths s_j s and the concentration parameter τ without significantly changing the distribution. This issue increases computational difficulty; we discuss our strategies for dealing with this challenge in Section 4.

3.2 Limiting behavior

In this section, we show that the Gaussian linear factor model is a limiting case of the Ellipsoid-Gaussian distribution. The following Lemma states that, as the concentration of a von Mises-Fisher distribution increases, the distribution approaches a degenerate Gaussian; a visualization of this lemma is included in the Appendices along with its proof.

Lemma 1. *Assume that $\eta \sim \text{vMF}(\mu, \tau)$. As $\tau \rightarrow \infty$, the quantity $\tau^{1/2}(\eta - \mu)$ converges in distribution to a multivariate Gaussian with mean 0 and covariance matrix $I_k - \mu\mu^T$, which is supported on the hyperplane perpendicular to μ .*

Using Lemma 1, we are able to show that as τ goes to infinity, (2) reduces to a Gaussian linear factor model with $(k - 1)$ -dimensional latent factors in \mathbb{R}^{k-1} .

Proposition 4. *Suppose we have a hyper-ellipsoid with axes represented by unit vectors u_1, \dots, u_k and semi-axis lengths $s_1 \geq s_2 \geq \dots \geq s_k \geq 0$, with $U = [u_1 \dots u_k]$ and $S = \text{diag}(s_1, \dots, s_k)$. Suppose x follows (2), with $\Lambda = \sqrt{\tau}US$. If we collapse the smallest axis by setting $s_k = 0$ and grow lengths of the remaining axes at rate $\sqrt{\tau}S$ while concentrating the latent factors $\eta \sim \text{vMF}(e_k, \tau)$ around $\mu = e_k$, model (2) converges in distribution to a Gaussian latent factor model with $k - 1$ latent factors and loading matrix $U_{-k}S_{-k}$ where $U_{-k} = [u_1 \dots u_{k-1}]$ and $S_{-k} = \text{diag}(s_1, \dots, s_{k-1})$, namely $x = c + \tilde{\Lambda}\tilde{\eta} + \epsilon$, where $\tilde{\eta} \sim N(0, I_{k-1})$, $\tilde{\Lambda} = U_{-k}S_{-k}$.*

4 Posterior computation

Our extensive experiments have shown that standard Markov chain Monte Carlo algorithms, such as the Gibbs sampler and Hamiltonian Monte Carlo, fail to perform adequately for posterior sampling in models involving Ellipsoid-Gaussian likelihoods. In this section, we describe the computational challenges and motivate the algorithm we choose—a hybrid of geodesic stochastic Nosé-Hoover thermostat (Liu et al., 2016) and adaptive Metropolis (Vihola, 2012). The detailed sampling procedures, including an extensive discussion of prior specification, gradient computation and an outline of the algorithm, can be found in the Appendices.

A brief comment is that samplers which rely on instantiating the latent variables $\{\eta_i\}$ tend to be subject to poor mixing; this includes Gibbs samplers. This is due to well known problems with Gibbs sampling in latent factor models, motivating pseudo marginal algorithms (Andrieu & Roberts, 2009; Beaumont, 2003; Vihola, 2012). We can bypass the need for pseudo marginal algorithms, which have also had poor performance in our experiments, due to the availability of a closed form likelihood marginalizing out the latent variables.

Marginalizing out the latent factors and using the resulting Ellipsoid-Gaussian likelihood in posterior sampling brings challenges. First, the term $\xi\{\tau\mu + \Lambda^T\Sigma^{-1}(x - c), \Lambda^T\Sigma^{-1}\Lambda/2\}$ needs to be approximated (Kume & Wood, 2005), but repeatedly applying such approximations becomes slow. Second, the gradient tends to change drastically with small changes in parameters, making it challenging to define efficient proposals. One failed example is the Barker proposal (Livingstone & Zanella, 2020). Even when proposal values are somewhat close to the current samples, the drastic changes in the gradient result in acceptance probability close to zero; to improve acceptance the algorithm adapts to propose tiny changes. The recently proposed transport Markov chain Monte Carlo (Duan, 2021) failed for similar reasons. Third, Gibbs-type updates lead to poor mixing, even with the latent factors marginalized out. For example, when we condition on the center c and the shape of the ellipsoid as determined by Λ , there is often not much uncertainty in μ , a parameter related to the mean direction of the data. As a result the chain tends to get stuck in a local mode. Fourth, μ is constrained to be on a sphere. A typical algorithm would require transforming μ to an unconstrained space \mathbb{R}^k . Specifically, to update μ , we update an unconstrained vector $\tilde{\mu}$ and map it back to μ with $\tilde{\mu}/\|\tilde{\mu}\|_2$. $\tilde{\mu}$, unfortunately, tends to move in the direction close to being perpendicular to the unit sphere centered at the origin, which translates into minimal movement in μ , as our experiments show. In addition, the update of the loading matrix is also not very efficient, even with the use of popular shrinkage priors, such as the Dirichlet-Laplace (Bhattacharya et al., 2015). This makes us wonder whether directly updating the axes directions and lengths can lead to faster convergence since the dimension of the parameter space would be drastically reduced.

A possible remedy to the first issue is to use stochastic gradient algorithms; a small subset of the data are involved in a given iteration, leading to dramatic speedup. By relying on a small step size, one can avoid the need for a Metropolis-Hastings correction (Y.-A. Ma et al., 2015), which circumvents the second issue. Also, by updating all the parameters in a single block, we address the third challenge. Our solution to the fourth problem is inspired by sampling schemes designed for distributions on manifolds embedded in Euclidean space with a known geodesic flow; see Byrne and Girolami (2013) and Liu et al. (2016) for more details.

Based on the above considerations, and on thorough experiments trying different algorithms, we use geodesic stochastic gradient Nosé-Hoover thermostats (Liu et al., 2016); we choose this dynamics because of the ease of tuning and robust performance. One weakness, however, is that all parameters share a single step size but the variances of their associated gradient are on vastly different scales. A discussion of our failed attempts to resolve this issue is included in the Appendices. Our solution is to add an additional transition kernel for the parameters that would benefit from a larger step size, such as Σ and τ ; robust adaptive Metropolis (Vihola, 2012) provides an effective way to define this transition kernel. We also face challenges in terms of prior specification due to non-identifiability; this is further discussed in the Appendices.

5 Simulation studies

5.1 Experiment setups

We compare to infinite mixtures of infinite factor analyzers (Murphy et al., 2020), abbreviated as mixtures of factor analyzers, and infinite Gaussian linear factor models to illustrate our ability to characterize multivariate distributions with curved dependence. We use the R package `IMIFA` (Murphy et al., 2021) for mixtures of factor analyzers and `infinitefactor` (Poworoznek, 2020) for Gaussian linear factor models. Both packages use Markov chain Monte Carlo.

We generate 1,000 data samples from each of the models specified in Section 5.2 and then compare performance in two different ways. First, we evaluate the log posterior predictive density on the test sets, which are set to be 5%, 10%, 15%, 20%, 30%, \dots , 90% of the simulated data samples. The estimated log posterior predictive density is $\sum_{i \in \text{test set}} 1/M \sum_{m=1}^M \log q(x_i; \theta^{(m)})$, where $q(x_i; \theta^{(m)})$ is the likelihood of the data evaluated at the m th draw $\theta^{(m)}$ from the posterior. Second, we randomly hold out 5% to 30% of the data entries and compare performance in predicting the hold-out sets using predictive MSE. The test sets and the hold-out sets differ in that the former corresponds to entire entries of certain observations and the latter corresponds to partial entries only.

As Ellipsoid-Gaussian, Gaussian linear factor models and mixtures of factor analyzers are all factor models, we require specification of the number of latent factors. For Ellipsoid-Gaussian, the number of latent factors is determined by WAIC (Watanabe, 2013). For mixtures of factor analyzers and Gaussian linear factor models, the number of latent factors is automatically determined in the packages we use. We use default initialization of all three methods; the details of initialization for Ellipsoid-Gaussian can be found in the Appendices. As Ellipsoid-Gaussian uses a stochastic gradient Monte Carlo algorithm, specification of a step size parameter is required. As is common practice for these algorithms, we choose a suitable step size from

$\{5 \times 10^{-4}, 10^{-4}, 5 \times 10^{-5}, 10^{-5}\}$ in a tuning phase.

5.2 Simulated data sets

In the simulation experiments, we generate three data sets from Ellipsoid-Gaussian distributions, two with curvature and one without. We also generate data from the hybrid Rosenbrock (Pagani et al., 2021), which was recently introduced as a benchmark to test the performance of Markov chain Monte Carlo on distributions with a curved and narrow shape. The density of a hybrid Rosenbrock random variable $x = (x_1, \dots, x_{n_2, n_1})$ is

$$\exp \left\{ -a_{ro}(x_1 - \nu)^2 - \sum_{j=1}^{n_2} \sum_{i=1}^{n_1} b_{ji}(x_{ji} - x_{j,i-1}^2)^2 \right\}, \quad (3)$$

where $a_{ro}, b_{ji} \in \mathbb{R}^+$. The settings of the simulated data sets are as follows:

- very curved in \mathbb{R}^{10} : $x_i = \Lambda \eta_i + \epsilon_i$, $\eta_i \sim \text{vMF}(\mu, 3)$, $\epsilon_i \sim \text{N}(0, 0.01I_{10})$, $k = 3$.
- shell shape in \mathbb{R}^3 : $x_i = \Lambda \eta_i + \epsilon_i$, $\eta_i \sim \text{vMF}(\mu, 5)$, $\epsilon_i \sim \text{N}(0, 0.01I_3)$, $k = 3$.
- approx. Gaussian in \mathbb{R}^6 : $x_i = \Lambda \eta_i + \epsilon_i$, $\eta_i \sim \text{vMF}(\mu, 30)$, $\epsilon_i \sim \text{N}(0, 0.4I_6)$, $k = 2$.
- Gaussian linear factor in \mathbb{R}^6 : $x_i = \Lambda \eta_i + \epsilon_i$, $\eta_i \sim \text{N}(0, I_3)$, $\epsilon \sim \text{N}(0, 0.01I_6)$, $k = 3$.
- hybrid Rosenbrock in \mathbb{R}^3 : $a_{ro} = 1$, $b = (30, 1)^T$, $\nu = 0$ in Equ. 3.

5.3 Simulation results

In these examples, mixtures of factor analyzers tend to perform comparably to Ellipsoid-Gaussian when the training set size is large, and the Gaussian linear factor model tends to perform the worst in the presence of curvature, as evidenced by the out-of-sample log posterior predictive density in Fig. 6. Other supporting figures can be found in the Appendices.

One interesting example is the very curved data in \mathbb{R}^{10} . Figure 6 shows that mixtures of factor analyzers are only able to perform comparably to the Gaussian linear factor model even when the training set size is large. For the examples Gaussian linear factor in \mathbb{R}^6 and approx. Gaussian in \mathbb{R}^6 , where the data can be approximated by a Gaussian distribution, the three methods perform equally well, though mixtures of factor analyzers experience a terrible run when the training set size is 500; see Fig. 6. As the training sample size decreases, the performance of mixtures of factor analyzers tends to be worse than that of Ellipsoid-Gaussian.

While the Gaussian linear factor model fails to capture curvature in the data sets (see Fig. 7c), its performance is surprisingly good in terms of MSE, which highlights limitations of the MSE at capturing departures from Gaussianity. In addition, the model tends to use more latent factors than the number of variables in the data, suggesting a lack of dimension reduction and interpretability. As expected, mixtures of factor analyzers also use too many components leading to spurious clusters, which is especially true when the model is fitted to small sample size data with missing entries; see the visualisation of the posterior predictive distribution in Fig. 7b.

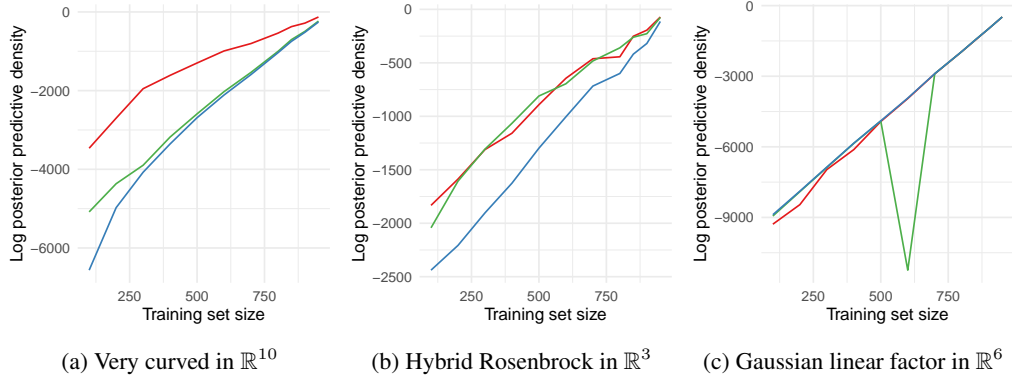


Figure 6: The log posterior predictive density of the test sets evaluated under each model as a function of the test set sizes, with red, blue and green corresponding to Ellipsoid-Gaussian, Gaussian linear factor models and mixtures of factor analyzers, respectively.

6 Real data applications

6.1 Horse mussel data

The horse mussel data can be found in the R package `dtr` (Weisberg, 2002), and contain measurements on 201 horse mussels taken from five sites in New Zealand in December 1984 (Camden, 1989). The measurements include shell width W , length L and height H , each in millimeters, and shell mass S and muscle mass M , each in grams. An interest of the study lies in predicting the muscle mass, the edible portion of the mussel, using other variables. The scatter plot matrix in Fig. 2b shows that the variables have curved relationships. We standardize the data such that each variable has mean zero and variance one. We choose step size $\epsilon = 5 \times 10^{-4}$ and $k = 3$ for Ellipsoid-Gaussian.

Applying cross validation in which we hold out up to 70% of the data, we find that Gaussian linear factor models are not competitive while Ellipsoid-Gaussian and mixtures of factor analyzers have similar fit out of sample. However, mixtures of factor analyzers are complex to interpret, in using three mixture components with each having up to four latent factors. This also leads to spurious clusters or outliers in the posterior predictive distribution; see Fig. 9b. In contrast, our Ellipsoid-Gaussian model has a linear factor structure simplifying interpretation. To illustrate this, we estimate the factor loadings structure by applying the MatchAlign algorithm (Poworoznek et al., 2021) to resolve rotational ambiguity and column label switching in Λ . The posterior mean of the resulting samples is visualized in Fig. 8a, where we see the muscle mass largely depends on a latent factor representing overall shell size. Figure 8b shows the relationship between the posterior mean of the muscle mass and the shell width holding the other covariates at their sample mean level: the muscle mass appears to be roughly constant when the shall length is less than 250mm and then increases linearly as shell length increases.

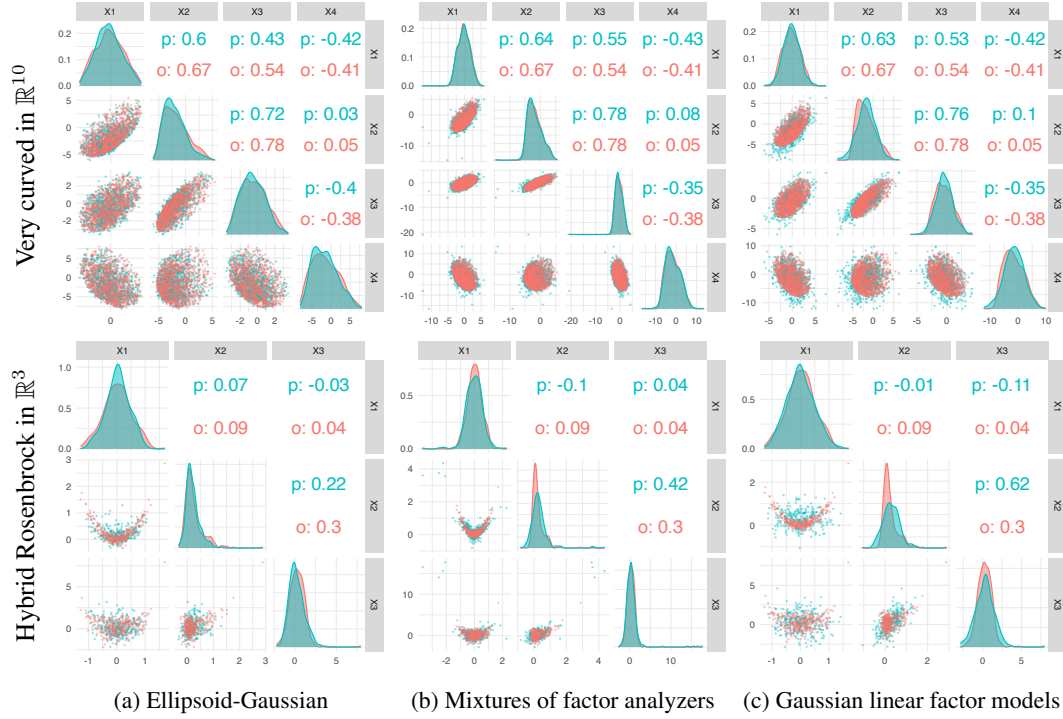


Figure 7: The scatter plot matrices of the posterior predictive (green) juxtaposed with the original data (red) for each method, where the models were fitted to the very curved data set in \mathbb{R}^{10} with 1000 observations and 20% random missingness (top row) and the hybrid Rosenbrock data in \mathbb{R}^3 with 300 observations (bottom row) respectively. Letters p and o stand for posterior predictive and original data respectively.

6.2 Air quality data

Urban atmospheric pollutants are believed to have contributed to an increasing incidence of respiratory illnesses. To monitor urban air quality, a multi-sensor device was placed in a polluted area in an Italian city and recorded hourly averaged responses, reflecting concentrations of CO, total nitrogen oxides (NO_x), nitrogen dioxide (NO_2) and O_3 (De Vito et al., 2008). The scatter plot matrix in Figure 9a shows that the variables have curved dependence. An interest of the study is to estimate benzene concentration using the four measurements, with the benzene reference concentration provided by a conventional fixed station (De Vito et al., 2008). The data set contains 8991 observations for each chemical. We normalize the data prior to analysis.

Figure 9a illustrates the posterior predictive distribution produced by the Ellipsoid-Gaussian, with the fitted marginal distributions matching those of the original data and capturing the curvature. The posterior predictive distribution produced by Gaussian linear factor models does not match the curvature in the data while that by mixtures of factor analyzers contain outliers. Gaussian linear factor model underfit, while mixtures of factor analyzers produce an overly complex

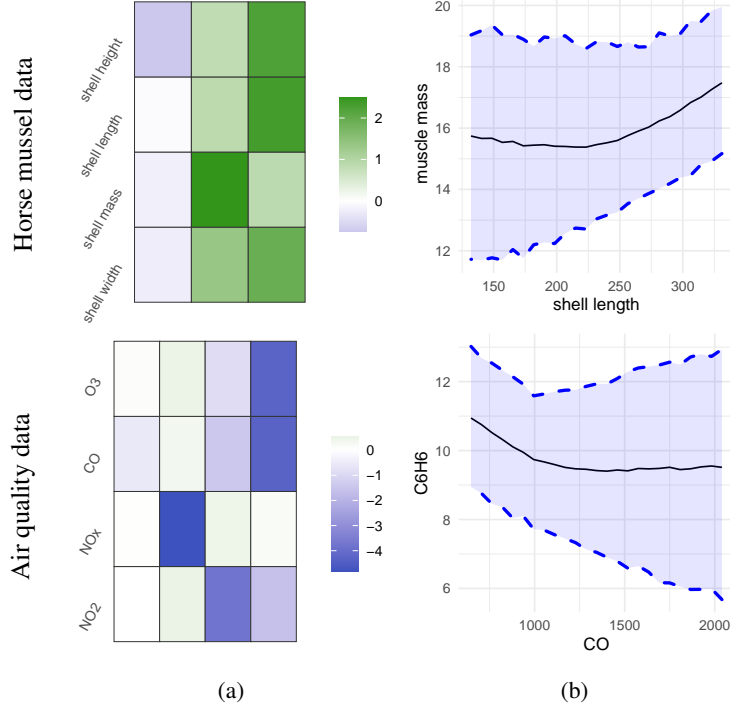


Figure 8: Results associated with Ellipsoid-Gaussian. Left: the posterior mean of the post-processed factor loadings of Λ . Right: the posterior mean (black) and the 95% credible band (blue ribbon) of muscle mass (top) and the benzene level (bottom) as a function of shell length and the CO level respectively, holding other covariates at their sample mean level.

fit with twenty-one components, each with up to four latent factors. Hence, we focus on the Ellipsoid-Gaussian as a good compromise between fit and interpretability.

Figure 8a visualizes the posterior mean of the post-processed loading matrix, suggesting the weighted average of O₃ and CO concentration as one of the important latent factors. Figure 8b shows the relationship between the expected benzene concentration and the CO concentration holding all other variables at their sample mean level; specifically, the benzene level tends to decrease as CO increases when the concentration of CO is less than 1000 mg/m³, but largely remains stable as the CO level continues to increase.

7 Discussion

In this article, we propose a simple and flexible von-Mises Fisher linear factor model to capture curved dependence in data, leading to a new class of Ellipsoid-Gaussian multivariate distributions. Simulating from the model results in points distributed about an ellipsoid, which is flexible enough to match curvature in many datasets. The use of a single factor loading matrix facilitates

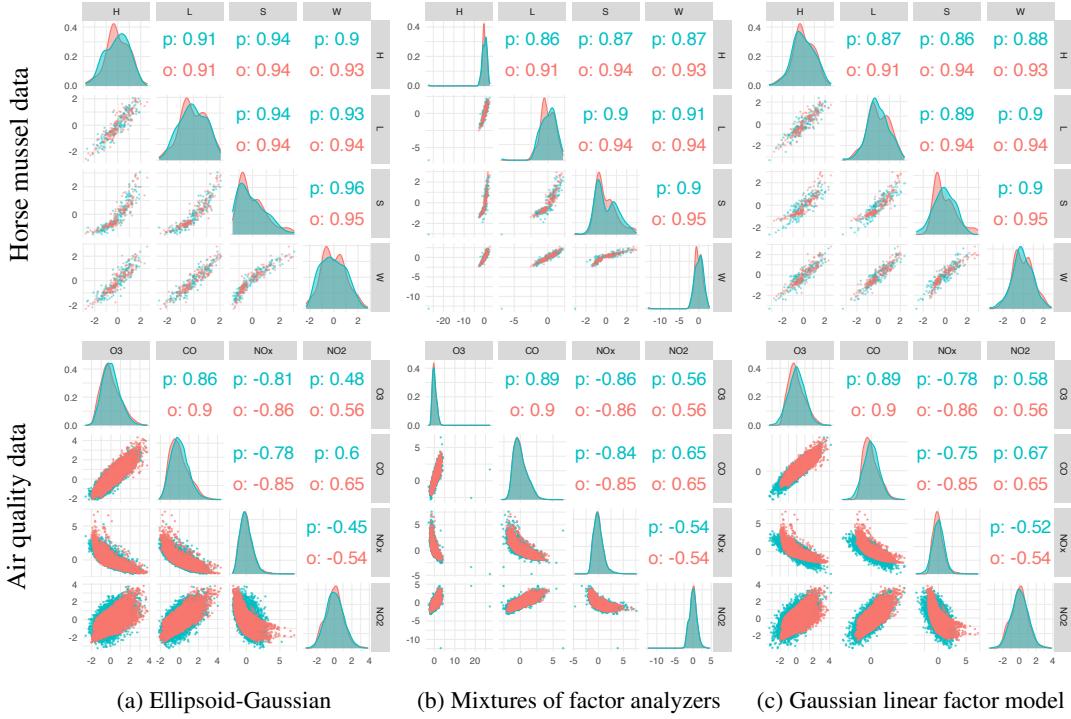


Figure 9: The scatter plot matrices of the posterior predictive (green) juxtaposed with the original data (red); the model was fitted to data sets with 20% in the hold-out sets. Letters p and o stand for posterior predictive and original data respectively.

dimension reduction and simple interpretation. In contrast, Gaussian linear factor models fail to characterize curvature and mixtures of factor analyzers are highly complex and can overfit the data, leading to spurious clusters and outliers in the posterior predictive.

In the absence of curved dependence in data, the model behaves like the routinely used Gaussian linear factor model, as we demonstrate both theoretically and empirically. We show how to marginalize out the latent factors and derive the density with respect to the Lebesgue measure. We also characterize various appealing properties of the distribution, such as that the marginal distribution of any sub-vector still follows an Ellipsoid-Gaussian.

There are a number of directions that would be interesting to pursue in future work. First, it is conceptually appealing to place shrinkage priors on the loadings, such as in Kowal, 2021. However, this leads to challenges in computation. Currently, we sample the axes directions U (i.e. the left singular vectors of Λ) and the axes lengths (i.e. the singular values of Λ). It is appealing to develop shrinkage priors for the axis directions to facilitate high-dimensional inferences, but the directions are constrained to the Stiefel manifold, making it unclear how to define appropriate priors. Second, efficiency of fitting Ellipsoid-Gaussian models is constrained by computation for approximating the pseudo-normalising constant. A faster but still reliable method for approximating this term would be helpful.

8 Acknowledgement

This work was partially supported by grants R01ES027498 and R01ES028804 of the National Institute of Environmental Health Sciences of the United States National Institutes of Health.

Appendices

In this section, we provide proofs for Propositions 1–4 and Lemma 1. We discuss challenges of prior specification specific to the Ellipsoid-Gaussian distribution, followed by gradient computation, sampling procedures, initialization of the sampler and imputation of latent factors. In the last part, we include additional results for the simulation study and real data applications.

A Proofs of propositions and lemmas

A.1 Proof of Proposition 1

Proof. 1. Let $w = \Lambda\eta$ and ϕ denote the pdf of ϵ . So $x = c + w + \epsilon$. We claim the density of x is

$$f_{\text{ellipsoid Gaussian}}(x) = \mathbb{E}_w [\phi(x - c - w)], \quad (4)$$

with respect to the Lebesgue measure in \mathbb{R}^p . Equation (4) can be simplified to be

$$\begin{aligned} & \mathbb{E}_\eta [\phi(x - c - \Lambda\eta)] \\ &= \int_{\mathcal{S}_{k-1}} \phi(x - c - \Lambda\eta) f_{\text{vMF}}(\eta) \mathcal{S}^{k-1}(d\eta) \\ &= \int_{\mathcal{S}_{k-1}} \left[(2\pi)^{-\frac{p}{2}} \frac{1}{\prod_{i=1}^p \sigma_i} \exp \left\{ -\frac{1}{2} (x - c - \Lambda\eta)^T \Sigma^{-1} (x - c - \Lambda\eta) \right\} \right] \times \\ & \quad \{ C_k(\tau) \exp(\tau \eta^T \mu) \} \mathcal{S}^{k-1}(d\eta) \end{aligned} \quad (5)$$

$$\begin{aligned} &= \frac{C_k(\tau)}{(2\pi)^{\frac{p}{2}} \prod_{i=1}^p \sigma_i} \exp \left\{ -\frac{1}{2} (x - c)^T \Sigma^{-1} (x - c) \right\} \times \\ & \quad \int_{\mathcal{S}_{k-1}} \underbrace{\exp \left\{ -\frac{1}{2} \eta^T (\Lambda^T \Sigma^{-1} \Lambda) \eta + (\tau \mu^T + (x - c)^T \Sigma^{-1} \Lambda) \eta \right\}}_{*} \mathcal{S}^{k-1}(d\eta) \end{aligned} \quad (6)$$

$$\begin{aligned} &= \frac{C_k(\tau)}{(2\pi)^{\frac{p}{2}} \prod_{i=1}^p \sigma_i} \exp \left\{ -\frac{1}{2} (x - c)^T \Sigma^{-1} (x - c) \right\} \\ & \quad \varsigma \left\{ \tau \mu + \Lambda^T \Sigma^{-1} (x - c), \frac{\Lambda^T \Sigma^{-1} \Lambda}{2} \right\}, \end{aligned}$$

where $*$ is the kernel of the Fisher-Bingham distribution with parameter $\kappa = \|\tau\mu + \Lambda^T \Sigma^{-1}(x - c)\|$, $\vartheta = \{\tau\mu + \Lambda^T \Sigma^{-1}(x - c)\} / \kappa$ and $A = \Lambda^T \Sigma^{-1} \Lambda / 2$. Now we show that the density of x is

$$f_{\text{ellipsoid Gaussian}}(x) = \mathbb{E}_w \{\phi(x - c - w)\}.$$

Recall that if \mathcal{U}, \mathcal{V} are finite Borel measures such that \mathcal{V} has a density g with respect to Lebesgue measure, then the convolution $\mathcal{U} * \mathcal{V}$ has density $g * \mathcal{U}$, as defined by

$$g * \mathcal{U}(x) = \int g(x - z) d\mathcal{U}(z). \quad (7)$$

In the special case where \mathcal{U} and \mathcal{V} are both probability measures, the convolution $\mathcal{U} * \mathcal{V}$ is the distribution of $Y + Z$, where Y, Z are independent random variables with marginal distributions \mathcal{U} and \mathcal{V} . Equation (7) can be rewritten as:

$$g * \mathcal{U}(x) = \int g(x - z) d\mathcal{U}(z) = \mathbb{E}g(x - Y),$$

where $x = c + w + \epsilon$ and ϵ has a density ϕ with respect to Lebesgue measure on \mathbb{R}^p . Hence the density of x is

$$f_{\text{ellipsoid Gaussian}}(x) = \mathbb{E}_w \{\phi(x - c - w)\}.$$

2. With $\Sigma = \sigma^2 I_p$, $\Lambda = r I_p$, and $k = p$, equation (6) can be simplified to

$$\begin{aligned} & \int_{S_{k-1}} \exp \left[-\frac{1}{2} \eta^T (\Lambda^T \Sigma^{-1} \Lambda) \eta + \{\tau\mu^T + (x - c)^T \Sigma^{-1} \Lambda\} \eta \right] \mathcal{S}^{k-1}(d\eta) \\ &= \int_{S_{k-1}} \exp \left[-\frac{r^2}{2\sigma^2} \eta^T \eta + \left\{ \tau\mu^T + \frac{r}{\sigma^2} (x - c)^T \right\} \eta \right] \mathcal{S}^{k-1}(d\eta) \\ &= \exp \left(-\frac{r^2}{2\sigma^2} \right) \int_{S_{k-1}} \underbrace{\left\{ \tau\mu^T + \frac{r}{\sigma^2} (x - c)^T \right\} \eta}_{**} \mathcal{S}^{k-1}(d\eta) \\ &= \exp \left(-\frac{r^2}{2\sigma^2} \right) \frac{1}{C_p(\|\tau\mu + \frac{r}{\sigma^2}(x - c)\|)}, \end{aligned}$$

where $**$ corresponds to a von-Mises Fisher distribution with concentration parameter $\tau^* = \|\tau\mu + \frac{r}{\sigma^2}(x - c)\|$ and mean direction $\mu^* = \tau\mu + \frac{r}{\sigma^2}(x - c) / \tau^*$. Hence, the part multiplied by $*$ in equation (6) can also simplified to be:

$$\frac{C_k(\tau)}{(2\pi\sigma^2)^{\frac{p}{2}}} \exp \left\{ -\frac{1}{2\sigma^2} (x - c)^T (x - c) \right\}.$$

The density of x is thus

$$\frac{C_k(\tau)}{(2\pi\sigma^2)^{\frac{p}{2}} C_p(\|\tau\mu + \frac{r}{\sigma^2}(x - c)\|)} \exp \left[-\frac{1}{2\sigma^2} \{(x - c)^T (x - c) + r^2\} \right],$$

with respect to the Lebesgue measure on \mathbb{R}^p , which coincides with the density of the Fisher-Gaussian kernel.

3. Let I denote a subset of the indices $\{1, \dots, p\}$ of a vector x , and x_I to be the vector of length $|I|$ containing the entries of x corresponding to the elements of I ; the matrix Λ_I represents the matrix with $|I|$ rows which are equal to the rows of Λ with indices in I . With this notation, we have $x_I = c_I + \Lambda_I \eta + \epsilon_I$, where $\epsilon_I \sim \mathcal{N}(0, \Sigma_I)$, $\Sigma_I = \text{diag}(\sigma_j, j \in I)$, $\eta \sim \mathcal{N}(\mu, \tau)$. This corresponds to the Ellipsoid-Gaussian distribution with density

$$f_{\text{EG}}(x_I) = \frac{C_k(\tau)}{(2\pi)^{\frac{|I|}{2}} \prod_{i \in I} \sigma_i} \exp \left\{ -\frac{1}{2} (x_I - c_I)^T \Sigma_I^{-1} (x_I - c_I) \right\} \\ \varsigma \left\{ \tau \mu + \Lambda_I^T \Sigma_I^{-1} (x_I - c_I), \frac{\Lambda_I^T \Sigma_I^{-1} \Lambda_I}{2} \right\}.$$

4.

$$\begin{aligned} \mathbb{E}(x) &= \mathbb{E}(c + w + \epsilon) \\ &= c + \mathbb{E}(\Lambda \eta) + \mathbb{E}\epsilon \\ &= c + \Lambda \mathbb{E}(\eta) \\ &= c + \Lambda \rho_k(\tau) \mu, \end{aligned}$$

where $\rho_k(\tau) = I_{k/2}(\tau)/I_{k/2-1}(\tau)$ and $I_r(\cdot)$ is the modified Bessel function of the first kind and order r .

5. The covariance of η is

$$\text{cov}(\eta) = \frac{\rho_k(\tau)}{\tau} I_k + \left\{ 1 - \frac{k}{\tau} \rho_k(\tau) - \rho_k^2(\tau) \right\} \mu \mu^T,$$

where $\rho_k(\tau)$ has the same definition as in 4. Hence,

$$\begin{aligned} \text{cov}(x) &= \text{cov}(w + \epsilon) \\ &= \text{cov}(w) + \text{cov}(\epsilon) \\ &= \Lambda \text{cov}(\eta) \Lambda^T + \Sigma \\ &= \frac{\rho_k(\tau)}{\tau} \Lambda \Lambda^T + \left\{ 1 - \frac{k}{\tau} \rho_k(\tau) - \rho_k^2(\tau) \right\} \Lambda \mu (\Lambda \mu)^T + \Sigma. \end{aligned}$$

□

A.2 Proof of Proposition 2

Proof. Let Γ be an arbitrary $k \times k$ orthogonal rotation matrix satisfying $\Gamma \Gamma^T = I_k$. Define $\tilde{\eta} = \Gamma \eta$, $\tilde{\Lambda} = \Lambda \Gamma^T$ and $\tilde{\mu} = \Gamma \mu$. The von-Mises Fisher density satisfies

$$f_{\text{vMF}}(\tilde{\eta}; \tilde{\mu}, \tau) = f_{\text{vMF}}(\eta; \mu, \tau).$$

Hence $x = c + \Lambda \eta + \epsilon = c + \tilde{\Lambda} \tilde{\eta} + \epsilon$, where $\tilde{\eta} \sim \text{vMF}(\tilde{\mu}, \tau)$.

□

A.3 Proof of Proposition 3

Lemma 2. *The moment generating function of the von-Mises Fisher distribution is*

$$M_{\text{vMF}}(t) = \frac{C_k(\tau)}{C_k(\|t + \tau\mu\|)}.$$

Proof. The moment generating function is given by

$$\begin{aligned} M_{\text{vMF}}(t) &= \mathbb{E} \left(e^{t^T \eta} \right) \\ &= \int C_k(\tau) \exp(t^T \eta + \tau \mu^T \eta) d\eta \\ &= C_k(\tau) \int \exp(\tilde{\tau} \tilde{\mu}^T \eta) d\eta \\ &= \frac{C_k(\tau)}{C_k(\tilde{\tau})}, \end{aligned}$$

where $\tilde{\tau} = \|t + \tau\mu\|$ and $\tilde{\mu} = (t + \tau\mu)/\tilde{\tau}$. □

of Proposition 3. An Ellipsoid-Gaussian random variable can be expressed in the form $x = c + \Lambda\eta + \epsilon$. Since the moment generating function of a sum of independent random variables is given by the product of moment generating functions, by Lemma 2

$$\begin{aligned} M_{\text{Ellipsoid-Gaussian}}(t) &= M_{c+\Lambda\eta}(t) M_{\epsilon}(t) \\ &= \exp(t^T c) M_{\text{vMF}}(\Lambda^T t) \exp\left(\frac{1}{2} t^T \Sigma t\right) \\ &= \exp\left(t^T c + \frac{1}{2} t^T \Sigma t\right) \frac{C_k(\tau)}{C_k(\|\Lambda^T t + \tau\mu\|)}. \end{aligned}$$

□

A.4 Proof of Lemma 1

J. Kent (1978) provided a partial proof to this Lemma, and here we provide a complete proof, along with an intuitive explanation in Fig. 10.

Proof. The characteristic function of $\text{vMF}_k(\mu, \tau)$, denoted by $\psi(t; \mu, \tau)$, is

$$\begin{aligned} \psi(t; \mu, \tau) &= C_k(\tau) \int_{S_k} \exp(it^T \eta + \tau \mu^T \eta) \nu_k(d\eta) \\ &= \frac{C_k(\tau)}{C_k(\|it + \tau\mu\|)}. \end{aligned}$$

Based on Henkel's expansion of the modified Bessel function of the first kind,

$$I_\nu(z) \sim (2\pi z)^{-1/2} e^z \{1 + O(|z|^{-1})\}, \quad |\arg z| < \frac{1}{2}\pi - \delta$$

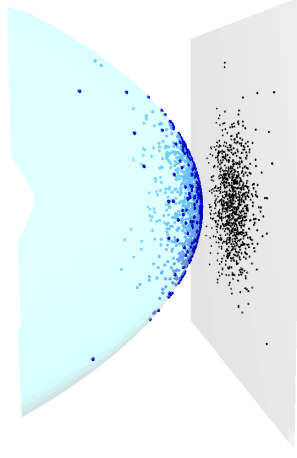


Figure 10: As the concentration of a von-Mises Fisher distribution increases, the distribution approaches a degenerate Gaussian, supported on the hyperplane perpendicular to μ .

as $z \rightarrow \infty$ with fixed v , where δ is an arbitrary fixed positive number. Hence,

$$\begin{aligned} \frac{C_k(z_1)}{C_k(z_2)} &= \frac{I_{k/2-1}(z_2)}{I_{k/2-1}(z_1)} \left(\frac{z_1}{z_2} \right)^{k/2-1} \\ &\sim \left(\frac{z_1}{z_2} \right)^{k/2} \exp(z_2 - z_1), \end{aligned}$$

as $z_1, z_2 \rightarrow \infty$ with both $|\arg z_1|$ and $|\arg z_2|$ smaller than $\frac{1}{2}\pi - \delta$. Letting $z_1 = \tau$ and $z_2 = \|i\tau^{\frac{1}{2}}t + \tau\mu\|$, z_2 can be rewritten as $\left(\tau^2 + 2\tau^{3/2}i \sum_{j=1}^k t_j \mu_j - \tau \sum_{j=1}^k t_j^2\right)^{\frac{1}{2}}$. As $\tau \rightarrow \infty$,

$$\left(\frac{z_1}{z_2} \right)^{k/2} \rightarrow 1,$$

and by a Taylor series expansion,

$$\begin{aligned} &\left(\tau^2 + 2\tau^{3/2}i \sum_{j=1}^k t_j \mu_j - \tau \sum_{j=1}^k t_j^2 \right)^{\frac{1}{2}} \\ &= \tau \left\{ 1 + i\tau^{-\frac{1}{2}} \sum_j t_j \mu_j - \frac{1}{2}\tau^{-1} \sum_j t_j^2 + \frac{1}{2}\tau^{-1} \left(\sum_j t_j \mu_j \right)^2 + O(\tau^{-3/2}) \right\}, \end{aligned}$$

we have

$$z_2 - z_1 = \tau \left\{ i\tau^{-\frac{1}{2}} \sum_j t_j \mu_j - \frac{1}{2}\tau^{-1} \sum_j t_j^2 + \frac{1}{2}\tau^{-1} \left(\sum_j t_j \mu_j \right)^2 + O(\tau^{-3/2}) \right\}.$$

Hence,

$$\begin{aligned}\exp(-i\tau^{\frac{1}{2}}t^T\mu)\psi(\tau^{\frac{1}{2}}t;\mu,\tau) &= \frac{C_k(\tau)}{C_k(\|i\tau^{\frac{1}{2}}t + \tau\mu\|)} \\ &\rightarrow \exp\left[-\frac{1}{2}\left\{\sum_j t_j^2 - \left(\sum_j t_j\mu_j\right)^2\right\}\right] \\ &= \exp\left\{-\frac{1}{2}t^T(I_k - \mu\mu^T)t\right\}.\end{aligned}$$

Hence, as $\tau \rightarrow \infty$, we have

$$\tau^{1/2}(\eta - \mu) \rightarrow N(0_k, I_k - \mu\mu^T).$$

To see this is a distribution on the hyperplane perpendicular to μ , consider random variable $Z \sim N_k(0_k, I_k)$, and note that

$$(I_k - \mu\mu^T)Z \sim N_k(0_k, I_k - \mu\mu^T),$$

since $I_k - \mu\mu^T$ is a perpendicular projection operator onto the space perpendicular to μ and is thus idempotent. $\tau^{1/2}(\eta - \mu)$ converges in distribution to Z as $\tau \rightarrow \infty$; by the continuous mapping theorem,

$$\{\tau^{1/2}(\eta - \mu)\}^T \mu \rightsquigarrow \{(I_k - \mu\mu^T)\}^T \mu = 0,$$

or equivalently,

$$\{\tau^{1/2}(\eta - \mu)\}^T \mu \rightsquigarrow 0, \tag{8}$$

where symbol \rightsquigarrow denotes convergence in distribution. \square

A.5 Proof of Proposition 4

Proof. If $s_k = 0$ and $\mu = e_k$, then we have $S = S(I_k - \mu\mu^T)$. $(I_k - \mu\mu^T)(\eta - \mu) = (I_k - \mu\mu^T)\eta$ and from Lemma 1 we know that $\sqrt{\tau}(I_k - \mu\mu^T)\eta \rightsquigarrow N(0, I_k - \mu\mu^T)$ as $\tau \rightarrow \infty$. Let $z \sim N(0, I_k)$ be a vector of standard normal latent factors and $z_{-k} \sim N(0, I_{k-1})$ be the first $k-1$ components. We can see that

$$\sqrt{\tau}S\eta = S\sqrt{\tau}(I_k - \mu\mu^T)\eta \rightsquigarrow S(I_k - \mu\mu^T)z = Sz$$

as $\tau \rightarrow \infty$, since $(I_k - \mu\mu^T)^2 = (I_k - \mu\mu^T)$. By decomposing into block matrices, we find

$$[U_{-k}u_k] \begin{bmatrix} S_{-k} & 0 \\ 0^T & 0 \end{bmatrix} \begin{bmatrix} z_{-k} \\ z_k \end{bmatrix} = [U_{-k}u_k] \begin{bmatrix} S_{-k}z_{-k} \\ 0 \end{bmatrix} = U_{-k}S_{-k}z_{-k}.$$

Thus as $\tau \rightarrow \infty$ we have

$$x_\tau \rightsquigarrow c + U_{-k}S_{-k}z_{-k} + \epsilon,$$

which is a Gaussian linear factor model with $k-1$ latent factors and factor loading matrix $U_{-k}S_{-k}$, as desired. \square

Table 1: Reference bounds for τ under different latent dimensions k

k	2	3	4	5	6	7	8	9	10
lower bound l_k	3	3	4	4	5	5	5	6	6
upper bound u_k	14	22	30	35	39	47	51	56	62

B Prior specification

B.1 Inference on the concentration parameter

As discussed in Section 3.1, a set of different hyper-ellipsoids, with each corresponding to a different concentration parameter τ , may be equally appropriate for the data at hand. Our strategy is to constrain τ , so that if we generate data with this τ the resulting data will be neither too concentrated nor too diffuse around an ellipsoid. We do not want the resulting data to be too diffuse because real data almost never wrap entirely around an ellipsoid. To this end, we put a lower bound on τ in the prior to eliminate almost-uniform distributions on the ellipsoid. We can also put an upper bound on τ because while real data can be very concentrated around an ellipsoid, there are other parameters we can adjust accordingly to fit the data well in the presence of a constraint on τ . In addition, for large τ_1 and τ_2 (greater than 100, for example), the distributions $\text{vMF}(\mu, \tau_1)$ and $\text{vMF}(\mu, \tau_2)$ are, for practical purposes, very similar. This can be formalized by examining the distances between the distributions for large τ .

To determine an appropriate set of bounds, we make use of the fact that the level curves of the von-Mises Fisher distribution on the surface of a unit sphere are rings radiating out from the mean direction. Due to the rotational property of the von-Mises Fisher distribution, these rings, which correspond to the angle between some unit vectors and the mean, are determined only by τ . To find a practical constraint on τ , we find the τ such that a certain percentage of the samples from the distribution are within a certain angle of μ . For example, to find a reasonable lower bound, we require that at least 95% of the generated points have an angle of at most $\pi/2$ with μ so that they do not wrap around the sphere; to find an upper bound, we require that at most 95% of the points lie within $\pi/7$ of μ so that they are not overly concentrated on the sphere. A side benefit of this approach is that the resulting bounds automatically adjust for the latent dimension. The resulting bounds can be found in Table 1.

B.2 Inference on the factor loading matrix

The non-identifiability of Λ , which encodes the axes directions and lengths of the underlying hyper-ellipsoid, poses challenges for computation. One natural idea is to put a strong shrinkage prior so that a narrower set of hyper-ellipsoids is favored. In fact, this kind of prior is frequently used in a variety of factor models, particularly for high-dimensional inference. Some examples of these shrinkage priors are the Dirichlet-Laplace prior of Bhattacharya et al. (2015) or the ordered spike-and-slab prior of Kowal (2021). Unfortunately, these priors do not assist with the inference for Λ in our model. In fact, we notice slower convergence when Λ is directly updated in comparison to when the axes directions (i.e. the left singular vectors of Λ) U and the axes lengths (i.e. the singular values of Λ) s_j 's are directly updated in many cases. These priors may also

come with some unintended side effects. Take the Dirichlet-Laplace prior as an example. When the penalization strength is too high, the prior strongly favors flat ellipsoids with axes parallel to the coordinate axes, which is often not consistent with the data.

One reason why directly updating the axes directions and lengths can lead to faster convergence is that the dimension of the parameter space is drastically reduced; as the k by k right singular vectors V of Λ are not identifiable, we can fix this parameter at the identity matrix and only update the left singular vectors and singular values. As a default choice, we choose a uniform prior on the Stiefel manifold for U .

On the other hand, we favor smaller ellipsoids through an appropriate prior on the axes lengths s_j 's, consistent with our previous choice of constraints on τ . As we constrain τ to be relatively small on the positive real line, we generally want small axis lengths, given that there is approximate non-identifiability when τ increases along with the axis lengths. As a prior for s_j that maintains this behavior, we choose a truncated Gaussian that is constrained to be positive and has small variance.

B.3 Prior specification

The discussion in Sections B.1 and B.2 leads to the following prior:

$$\begin{aligned} c &\sim \mathcal{N}(c_0, \sigma_c^2 I_p), \\ \tau &\sim \text{Gamma}(a, b) \mathbb{1}(\mathfrak{l}_k, \mathfrak{u}_k), \\ \mu &\sim \text{vMF}(\mu_0, \tau_0), \\ \sigma_j^2 &\sim \mathcal{N}(0, \sigma_0^2) \mathbb{1}(0, \infty), \quad j = 1, \dots, p \\ U &\sim \text{Unif}(V_k(\mathbb{R}^p)), \\ s_l &\sim \mathcal{N}(0, \sigma_s^2), \quad l = 1, \dots, k \end{aligned}$$

where $V_k(\mathbb{R}^p) = \{A \in \mathbb{R}^{p \times k} : A^T A = I_k\}$, and \mathfrak{l}_k and \mathfrak{u}_k are the lower and upper bounds for τ at latent dimension k . A set of reference bounds is provided in Table 1 and code to determine them is also provided in case a different constraint is preferred. We place a truncated Gaussian prior on the noise variance σ_j because we favor a fit with small noise. For μ , if a uniform prior on the unit sphere is desired, one can set $\tau_0 = 0$. For τ , we set $a = 5, b = 1$ to favor a relatively small τ value, representing a fit with curvature. c_0 and μ_0 are set to be the initialization of c and μ . Results are generally not sensitive to the choice of the prior parameters.

C Gradient computation

C.1 Notation and parameter transformation

Let $\theta = (c, \tau, \Lambda, \mu, \Sigma)$. Denote the prior for θ by $\pi_0(\theta)$ and the likelihood by $\pi(x \mid \theta)$. Let precision $1/\sigma_j^2$ be ω_j^2 . Given a data set $\mathcal{D} = \{x_i\}_{i=1}^N$, a stochastic gradient Monte Carlo algorithm draws a random subset \mathcal{S} of \mathcal{D} to build the stochastic gradient $\nabla_\theta \mathcal{G}(\theta) := -\nabla_\theta \log \pi_0(\theta) - N/|\mathcal{S}| \sum_{x \in \mathcal{S}} \nabla_\theta \log \pi(x \mid \theta)$. Using a gradient-based method, parameters must be unconstrained

Table 2: The parameters involved in the sampler

Original parameter θ	Parameter being updated θ'
c	c
τ	$\tilde{\tau} := \text{logit} \left(\frac{\tau - \mathbf{l}_k}{\mathbf{u}_k - \mathbf{l}_k} \right)$
U	U
s_l	$\tilde{s}_l := \log(s_l)$
μ	μ
σ_j^2	$\tilde{\sigma}_j := \log(1/\sigma_j^2)$

on the embedded manifold for ease of updates; this means we must transform several of our parameters. We update $\text{logit} \{(\tau - \mathbf{l}_k)/(\mathbf{u}_k - \mathbf{l}_k)\}$, $\log(1/\sigma_j^2)$ and $\log(s_l)$ instead of τ , σ_j^2 and s_l because the former parameters lie on the real line. That is, the set of parameters we are directly updating is

$$\theta' := \{c, \text{logit} \{(\tau - \mathbf{l}_k)/(\mathbf{u}_k - \mathbf{l}_k)\}, U, \{\log(s_l) : l = 1, \dots, k\}, \mu, \{\log(\omega_j^2) : j = 1, \dots, p\}\}.$$

Refer to Table 2 for a summary.

In the next sections, we present the gradient associated with these parameters. We use subscripts $j\cdot$ and $\cdot j$ to represent the j th row and column of a matrix respectively. For ease of representation, we denote $\tau\mu + \Lambda^T \Sigma^{-1}(x - c)$ and $\text{vec}(\Lambda^T \Sigma^{-1} \Lambda/2)$ by $g_1(x)$ and g_2 respectively. In addition, any vector (including gradient) is represented as a column vector.

C.2 Gradient from the likelihood

The gradient includes contributions from both the likelihood and the prior. For both parts, we need to first compute the gradient w.r.t θ and then apply the chain rule of differentiation. To this end, we need the following gradient:

$$\begin{aligned} \nabla_{\tilde{\tau}} \tau &= (\mathbf{u}_k - \mathbf{l}_k) \frac{\exp(\tilde{\tau})}{\{1 + \exp(\tilde{\tau})\}^2}, \\ \nabla_{\tilde{\sigma}_j} \omega_j^2 &= \omega_j^2, \\ \nabla_{\log(s_j)} \Lambda_{\cdot j} &= s_l U_{\cdot j}, \\ \nabla_{U_{\cdot j}} \Lambda_{\cdot j} &= (s_j, \dots, s_j)^T. \end{aligned}$$

Next, we discuss the gradient w.r.t θ from the likelihood. The log-likelihood of x can be written

as:

$$\begin{aligned}
\log \pi(x \mid \theta) &= \log \pi(x \mid \theta') \\
&= \log C_k(\tau) - \sum_{j=1}^p \log \sigma_j - \frac{1}{2}(x - c)^T \Sigma^{-1}(x - c) + \\
&\log \xi \left\{ \tau \mu + \Lambda^T \Sigma^{-1}(x - c), \frac{\Lambda^T \Sigma^{-1} \Lambda}{2} \right\} + \text{const.}
\end{aligned}$$

Since the pseudo-normalising constant ξ can only be approximated, the associated gradient must also be approximated, for which we use Richardson's extrapolation, an accurate numerical differentiation method, implemented by the R package `numDeriv` (Gilbert & Varadhan, 2019). We first present gradient w.r.t a single observation x :

$$\begin{aligned}
\nabla_\tau \log \pi(x \mid \theta) &= \nabla_\tau \log C_k(\tau) - \nabla_{g_1} \log \xi(g_1, g_2)^T \mu. \\
\nabla_\mu \log \pi(x \mid \theta) &= \tau \nabla_{g_1} \log \xi(g_1, g_2). \\
\nabla_c \log \pi(x \mid \theta) &= \Sigma^{-1}(x - c) - \Sigma^{-1} \Lambda \nabla_{g_1} \log \xi(g_1, g_2). \\
\nabla_{\omega_j^2} \log \pi(x \mid \theta) &= 0.5/\omega_j^2 - 0.5(x_{\cdot j} - c_j)^2 + \\
&\quad (x_{\cdot j} - c_j) \nabla_{g_1} \log \xi(g_1, g_2)^T \Lambda_{j\cdot} + \nabla_{g_2} \log \xi(g_1, g_2)^T \text{vec}(\Lambda_{j\cdot} \Lambda_{j\cdot}^T)/2. \\
\nabla_{\text{vec}(\Lambda)} \log \pi(x \mid \theta) &= \{I_k \otimes \Sigma^{-1}(x - c)\} \nabla_{g_1} \log \xi(g_1, g_2) + \\
&\quad \{K(p, k)^T (\Sigma^{-1} \Lambda \otimes I_k) + (I_k \otimes \Sigma^{-1} \Lambda)\} \nabla_{g_2} \log \xi(g_1, g_2),
\end{aligned}$$

where $g_1 = g_1(x)$, $x_{\cdot j}$ is the j th variable of x and $K(p, k)$ is a pk by pk commutative matrix such that $K(p, k) \text{vec}(\Lambda) = \text{vec}(\Lambda^T)$.

Updating with the subset \mathcal{S} , the gradient becomes

$$\begin{aligned}
\nabla_\tau \sum_{x \in \mathcal{S}} \log \pi(x \mid \theta) &= |\mathcal{S}| \nabla_\tau \log C_k(\tau) - \sum_{x \in \mathcal{S}} \nabla_{g_1(x)} \log \xi(g_1(x), g_2)^T \mu. \\
\nabla_\mu \sum_{x \in \mathcal{S}} \log \pi(x \mid \theta) &= \tau \sum_{x \in \mathcal{S}} \nabla_{g_1(x)} \log \xi(g_1(x), g_2). \\
\nabla_c \sum_{x \in \mathcal{S}} \log \pi(x \mid \theta) &= \sum_{x \in \mathcal{S}} \Sigma^{-1}(x - c) - \Sigma^{-1} \Lambda \nabla_{g_1(x)} \log \xi(g_1(x), g_2). \\
\nabla_{\omega_j^2} \sum_{x \in \mathcal{S}} \log \pi(x \mid \theta) &= 0.5|\mathcal{S}|/\omega_j^2 - \sum_{x \in \mathcal{S}} 0.5(x_{\cdot j} - c_j)^2 + \\
&\quad \sum_{x \in \mathcal{S}} (x_{\cdot j} - c_j) \nabla_{g_1(x)} \log \xi(g_1(x), g_2)^T \Lambda_{j\cdot} + \\
&\quad \sum_{x \in \mathcal{S}} \nabla_{g_2} \log \xi(g_1(x), g_2)^T \text{vec}(\Lambda_{j\cdot} \Lambda_{j\cdot}^T)/2. \\
\nabla_{\text{vec}(\Lambda)} \sum_{x \in \mathcal{S}} \log \pi(x \mid \theta) &= \sum_{x \in \mathcal{S}} \{I_k \otimes \Sigma^{-1}(x - c)\} \nabla_{g_1(x)} \log \xi(g_1(x), g_2) + \\
&\quad \{K(p, k)^T (\Sigma^{-1} \Lambda \otimes I_k) + (I_k \otimes \Sigma^{-1} \Lambda)\} \sum_{x \in \mathcal{S}} \nabla_{g_2} \log \xi(g_1(x), g_2).
\end{aligned}$$

Then apply the chain rule to find the gradient w.r.t θ' .

C.3 Gradient from the prior distribution

Next we discuss the gradient contributions from the prior distribution. The prior distribution is defined in Section B.3 in terms of θ . Since θ' is the parameter being updated, we need to find the prior distribution of θ' , denoted by $\pi_0(\theta')$, from $\pi_0(\theta)$, which involves the Jacobian term $J(\theta') = |\partial\theta/\partial\theta'|$. Transformation of random variable gives $\log \pi_0(\theta') = \log \pi_0(\theta) + \log J(\theta')$. Therefore, we have the following relationship

$$\nabla_{\theta'} \log \pi_0(\theta') = (\partial\theta/\partial\theta') \nabla_{\theta} \{\log \pi_0(\theta) + \log J(\theta')\}. \quad (9)$$

To find (9), we first find $\nabla_{\theta} \log \pi_0(\theta)$:

$$\begin{aligned} \nabla_{c_j} \log \pi_0(\theta) &= -(c_j - c_{0j})/\sigma_c^2, \\ \nabla_{\mu} \log \pi_0(\theta) &= \tau_0 \mu_0, \\ \nabla_{\tau} \log \pi_0(\theta) &= (a - b)/\tau - b, \\ \nabla_{\sigma_j^2} \log \pi_0(\theta) &= -\sigma_j^2/\sigma_0^2, \\ \nabla_U \log \pi_0(\theta) &= 0, \\ \nabla_{s_l} \log \pi_0(\theta) &= -s_l/\sigma_s^2. \end{aligned}$$

Then we add a logged Jacobian term and apply the chain rule as defined in (9) to find the gradient w.r.t the parameter θ' . Some details are as follows.

1. τ : Recall $\tilde{\tau} = \text{logit} \left(\frac{\tau - \mathbf{l}_k}{\mathbf{u}_k - \mathbf{l}_k} \right)$. $\frac{d\tau}{d\tilde{\tau}} = (\mathbf{u}_k - \mathbf{l}_k) \frac{\exp(\tilde{\tau})}{\{1 + \exp(\tilde{\tau})\}^2}$. $\log \pi_0(\tilde{\tau}) = \log \pi_0(\tau) + \log J(\tilde{\tau})$, where $J(\tilde{\tau}) = |\frac{d\tau}{d\tilde{\tau}}|$. It is easy to find that $J(\tilde{\tau}) = \frac{d\tau}{d\tilde{\tau}}$, and $\nabla_{\tilde{\tau}} \log J(\tilde{\tau}) = \frac{1 - \exp(\tilde{\tau})}{1 + \exp(\tilde{\tau})}$. In addition, by chain rule, $\nabla_{\tilde{\tau}} \log \pi_0(\tau) = \nabla_{\tau} \log \pi_0(\tau) \frac{d\tau}{d\tilde{\tau}}$. Hence, $\nabla_{\tilde{\tau}} \log \pi_0(\theta') = \nabla_{\tilde{\tau}} \log \pi_0(\theta) + \nabla_{\tilde{\tau}} \log J(\tilde{\tau}) = \nabla_{\tau} \log \pi_0(\theta) (\mathbf{u}_k - \mathbf{l}_k) \frac{\exp(\tilde{\tau})}{\{1 + \exp(\tilde{\tau})\}^2} + \frac{1 - \exp(\tilde{\tau})}{1 + \exp(\tilde{\tau})}$.
2. ω_j^2 : Recall $\tilde{\sigma}_j = \log \omega_j^2 = -\log \sigma_j^2$. For ease of demonstration, we drop index j for now. $\frac{d\sigma^2}{d\tilde{\sigma}} = -\exp(-\tilde{\sigma})$. $\log \pi_0(\tilde{\sigma}) = \log \pi_0(\sigma^2) + \log J(\tilde{\sigma})$, where $J(\tilde{\sigma}) = |\frac{d\sigma^2}{d\tilde{\sigma}}| = \exp(-\tilde{\sigma})$. In addition, by chain rule, $\nabla_{\tilde{\sigma}} \log \pi_0(\sigma^2) = \nabla_{\sigma^2} \log \pi_0(\sigma^2) \frac{d\sigma^2}{d\tilde{\sigma}}$. Hence, $\nabla_{\tilde{\sigma}} \log \pi_0(\theta') = \nabla_{\tilde{\sigma}} \log \pi_0(\theta) + \nabla_{\tilde{\sigma}} \log J(\tilde{\sigma}) = -\nabla_{\sigma^2} \log \pi_0(\theta) \exp(-\tilde{\sigma}) - 1$.

To summarise, the resulting prior gradient is as follows:

$$\begin{aligned} \nabla_{c_j} \log \pi_0(\theta') &= -(c_j - c_{0j})/\sigma_c^2, \\ \nabla_{\mu} \log \pi_0(\theta') &= \tau_0 \mu_0, \\ \nabla_{\tilde{\tau}} \log \pi_0(\theta') &= \{(a - b)/\tau - b\} (\mathbf{u}_k - \mathbf{l}_k) \frac{\exp(\tilde{\tau})}{\{1 + \exp(\tilde{\tau})\}^2} + \frac{1 - \exp(\tilde{\tau})}{1 + \exp(\tilde{\tau})}, \\ \nabla_{\tilde{\sigma}_j} \log \pi_0(\theta') &= -\exp(-2\tilde{\sigma}_j)/\sigma_0^2 - 1. \\ \nabla_U \log \pi_0(\theta') &= 0, \\ \nabla_{\log(s_l)} \log \pi_0(\theta') &= -s_l^2/\sigma_s^2 - 1. \end{aligned}$$

For each parameter, the gradient is a sum of the gradient from the likelihood and its prior distribution.

D Sampling algorithm

D.1 Sampling procedures

In this section, we outline the sampling procedures, which involve geodesic stochastic gradient Nosé-Hoover thermostat (Liu et al., 2016) and robust adaptive Metropolis algorithm (Vihola, 2012) at every iteration, in Algorithm 2. For notation brevity, the algorithms are abbreviated as gSGNHT and ramcmc respectively in Algorithm 2.

The dynamics of the geodesic algorithm is defined in Liu et al. (2016). We use a symmetric splitting integrator scheme, which leads to more accurate sample draws and a solution that depends on the Riemann metric tensor only through the geodesic flow. The sampling procedure is provided in Algorithm 1.

Good default choices of the tuning parameters are $A = 0.1$, $\epsilon = 5 \times 10^{-4}$ for the geodesic algorithm and $L = 10$, $\gamma = 2/3$ and the coerced acceptance rate $\alpha^* = 23.4\%$ for robust adaptive Metropolis algorithm.

Output: $\{\theta^{(t)} : t = 1, \dots, T\}$

- 1 Randomly initialize $\theta^{(0)}$
- 2 Sample $v^* \sim N(0, I)$, project $v^{(0)} \leftarrow \mathcal{P}(\theta^{(0)})v^*$ and set $\xi_{(0)} \leftarrow C$
- 3 **for** $t = 1, \dots, T$ **do**
- 4 Sample a subset \mathcal{S} for computing $\nabla_{\theta'} \mathcal{G}_{\mathcal{H}}(\theta')$.
 $(x_0, v_0, \xi_0) \leftarrow (x^{(t-1)}, v^{(t-1)}, \xi^{(t-1)})$
- 5 **for** $l = 1, \dots, L$ **do**
- 6 A: Update $(\theta^*, v^*) \leftarrow (x_{l-1}, v_{l-1})$ by the geodesic flow for time step $\epsilon/2$,
 $\xi^* \leftarrow \xi_{l-1} + (\frac{1}{m} v_{l-1}^T v_{l-1} - 1)\epsilon/2$
- 7 B: $v^* \leftarrow \exp\{-\xi^* \frac{\xi_n}{2}\} v^*$
- 8 O: $v^* \leftarrow v^* + \mathcal{P}(\theta^*) \cdot [-\nabla_{\theta'} \mathcal{G}_{\mathcal{H}}(\theta^*)\epsilon + N(0, (2A - \epsilon_n V(\theta^*))\epsilon_n)]$
- 9 B: $v^* \leftarrow \exp\{-\xi^* \frac{\xi_n}{2}\} v^*$
- 10 A: Update $(\theta_l, v_l) \leftarrow (\theta^*, v^*)$ by the geodesic flow for time step $\epsilon/2$,
 $\xi_l \leftarrow \xi^* + (\frac{1}{m} v^{*T} v^* - 1)\frac{\epsilon}{2}$
- 11 $(\theta^{(t)}, v^{(t)}, \xi^{(t)}) \leftarrow (\theta_L, v_L, \xi_L)$, and no Metropolis-Hasting correction step

Algorithm 1: Sampling steps of geodesic Nosé-Hoover thermostat (Liu et al., 2016)

D.2 Initialization

We use subscript *init* to represent the initial values of the parameters. We initialize the chain with $\tau_{init} = 5$ and the noise variance at a small value with $\Sigma_{init} = \text{diag}(0.1, \dots, 0.1)$ to facilitate identification of the underlying ellipsoid.

Let the principal components of the (centered) data to be \mathfrak{U} . We initialize the axes directions \mathcal{U}_{init} to be the first k principal components ordered by the associated standard deviation in decreasing order. To find the center c_{init} , we first rotate the data so that the new coordinate axes are parallel to the principal components \mathfrak{U} , then use the mid points of the ranges in each di-

Output: samples from the posterior distribution $\{\theta^{(t)} : t = 1, \dots, T\}$

- 1 Randomly initialize $\theta^{(0)}$
- 2 Sample $v^* \sim N(0, I)$ and project $v^{(0)} \leftarrow \Lambda(\theta^{(0)})v^*$. $\xi_{(0)} \leftarrow C$
- 3 **for** $t = 1, \dots, T$ **do**
 - ▷ gSGNHT: joint update of θ'
 - 4 Follow the steps 4, 5, 6, 7, 8, 9, 10 and 11 of Algorithm 1
 - ▷ ramcmc: joint update of $\iota := (\tilde{\tau}, \tilde{\sigma}_1, \dots, \tilde{\sigma}_p)$
 - 5 Compute $\iota^* = \iota^{(t)} + M_{t-1}W_t$, where W_t is a random vector from a standard multivariate Gaussian distribution
 - 6 With probability $\alpha_t := \min\{1, \pi(\iota^* | \mathcal{D})/\pi(\iota^{(t)} | \mathcal{D})\}$, the proposal is accepted and $\iota^{(t)} = \iota^*$; otherwise, the proposal is rejected
 - 7 Compute the lower-diagonal matrix M_t with positive diagonal elements satisfying the equation

$$M_t M_t^T = M_{t-1} \left(I + t^{-\gamma} (\alpha_t - \alpha^*) \frac{W_t W_t^T}{\|W_t\|^2} \right) M_{t-1}^T,$$

where $\gamma \in (1/2, 1]$, and α^* is the coerced acceptance rate

Algorithm 2: The posterior sampler for Ellipsoid-Gaussian

mension as an initial estimate of the center, which is then transformed back to the Cartesian coordinate system to be c_{init} . To initialize the axes lengths, we first center the data by using the estimated center c_{init} so that the data are centered around the origin, then map the data by U_{init}^T to the coordinate space of the first k principal components, and calculate the average distances to the origin along each coordinate axis as the initial estimates of the axes lengths. To initialize μ , we estimate $S_{init}\mu_{init}$ based on the first moment of the Ellipsoid-Gaussian distribution and invert the quantity by the initial value of S , where $S = \text{diag}(s_1, \dots, s_k)$. Specifically, $S_{init}\mu_{init} = U_{init}^T (\bar{x} - c_{init}) / \rho_k(\tau_{init})$. This can be solved for μ_{init} , so we then set the initial value μ_{init} to be the normalised version of $U_{init}^T (\bar{x} - c_{init}) / \rho_k(\tau_{init}) \oslash s_{init}$, where $s = (s_1, \dots, s_k)^T$.

D.3 Imputation of the latent factors

While our posterior sampler relies on marginalizing out the latent factors, sampling the latent factors can be of interest. To impute the latent factors for observation i , we simply add an additional step of drawing from $\eta_i | x_i, \theta_i$ at every Markov chain Monte Carlo iteration. Although $\eta_i | x_i, z_i$ follows a Fisher-Bingham distribution and there are dedicated algorithms to sample from this distribution in the literature (Hoff, 2009; J. T. Kent et al., 2013), our experiments show poor performance for these algorithms. Instead, we take advantage of the fact that in our setting, the Fisher-Bingham tends to be highly concentrated, motivating a von-Mises Fisher with high concentration (e.g. 30) centered at the current value as the proposal distribution for a Metropolis-Hasting update.

Specifically, the full conditional of latent factor η_i is Fisher-Bingham($\bar{\tau}_i, \bar{\mu}_i, \bar{A}_i$), where $\bar{\tau}_i = \|\tau\mu + \Lambda^T \Sigma^{-1}(x_i - \mathbf{c})\|$, $\bar{\mu}_i = \{\tau\mu + \Lambda^T \Sigma^{-1}(x_i - \mathbf{c})\} / \bar{\tau}_i$ and $\bar{A}_i = \Lambda^T \Sigma^{-1} \Lambda / 2$. In our

experiments, we choose the concentration parameter to be 30 and perform the transition for 20 times at every iteration for improved convergence.

D.4 Other comments on the sampling algorithm

As we discussed in Section 4, geodesic stochastic gradient Nosé-Hoover thermostat suffers from the problem of using a single step size for all parameters, whose associated gradients are on vastly different scales. One intuitive solution is to use a preconditioner which guarantees a larger step size in directions with less curvature and a smaller step size in directions with more curvature. This strategy has been widely used in stochastic gradient descent algorithms and some gradient-based sampling algorithms such as Hamiltonian Monte Carlo. Unfortunately, the position where a preconditioner assumes is taken by the Riemann metric tensor G . We can see this by understanding the algorithm dynamics in Liu et al., 2016.

An alternative solution is to add an additional transition kernel for parameters that would benefit from taking a larger step. Such parameters include τ and Σ , and the robust adaptive Metropolis algorithm (Vihola, 2012) provides an elegant recipe for this additional transition kernel.

E Experiment results

E.1 Simulation results

In this section, we provide additional results of the simulation study. This includes the out-of-sample log posterior predictive density (Fig. 11) and scatter plot matrices of the posterior predictive (Fig. 13) for the data sets not displayed in the paper. Imputing the hold-out entries by mixtures of factor analyzers is extremely slow to the extent of being computationally intractable for moderate dimensional (e.g. the very curved example in R^{10}) or large (e.g. the air quality data with 9,000 observations) datasets. Recall the settings of the simulations are as follows:

- Very curved in \mathbb{R}^{10} : $x_i = \Lambda\eta_i + \epsilon_i$, $\eta_i \sim \text{vMF}(\mu, 3)$, $\epsilon_i \sim \text{N}(0, 0.01I_{10})$, $k = 3$.
- Shell shape in \mathbb{R}^3 : $x_i = \Lambda\eta_i + \epsilon_i$, $\eta_i \sim \text{vMF}(\mu, 5)$, $\epsilon_i \sim \text{N}(0, 0.01I_3)$, $k = 3$.
- Approx. Gaussian in \mathbb{R}^6 : $x_i = \Lambda\eta_i + \epsilon_i$, $\eta_i \sim \text{vMF}(\mu, 30)$, $\epsilon_i \sim \text{N}(0, 0.4I_6)$, $k = 2$.
- Gaussian linear factor in \mathbb{R}^6 : $x_i = \Lambda\eta_i + \epsilon_i$, $\eta_i \sim \text{N}(0, I_3)$, $\epsilon \sim \text{N}(0, 0.01I_6)$, $k = 3$.
- Hybrid Rosenbrock in \mathbb{R}^3 : $a_{ro} = 1$, $b = (30, 1)^T$, $\nu = 0$ in Equ. 3.

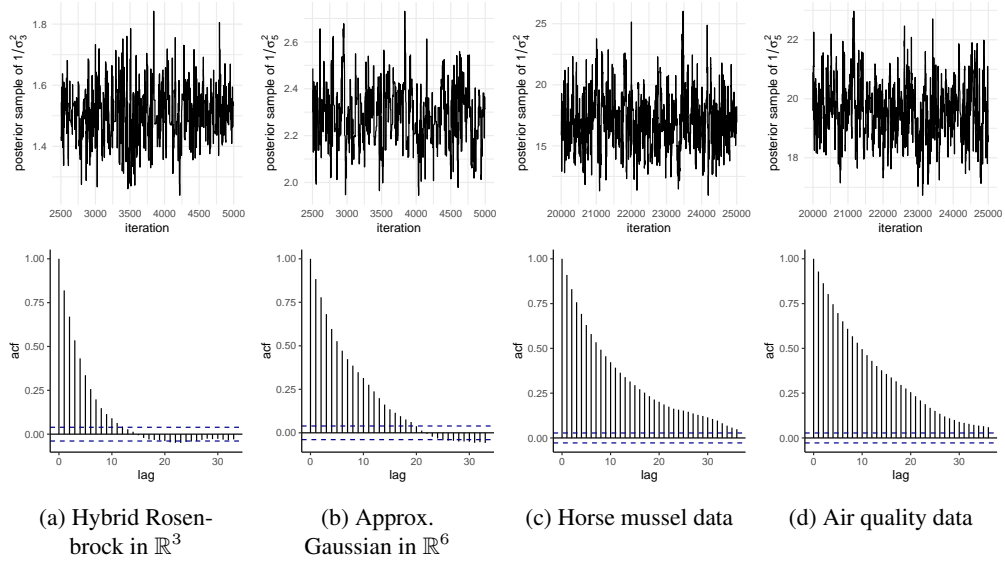


Figure 12: The trace plot (top row) and the auto correlation function plot (bottom row) of some precision parameters for the simulated and real data sets.

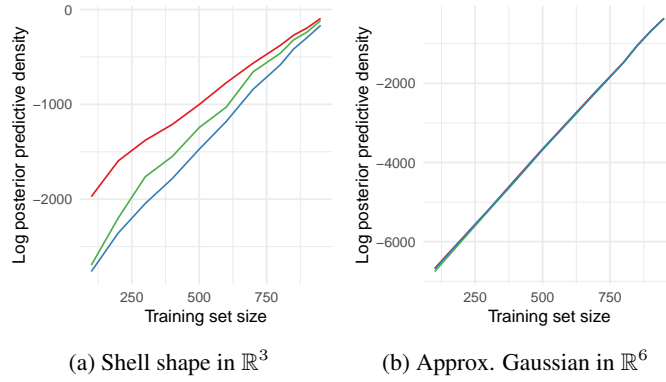


Figure 11: The log posterior predictive density of the test sets evaluated under each model as a function of the test set sizes, with red, blue and green corresponding to Ellipsoid-Gaussian, Gaussian linear factor models and mixtures of factor analyzers, respectively. In Fig. 11b the three curves are exactly overlapping, indicating the performance of the three methods is comparable.

E.2 Application results

In Fig. 14, we visualize the relationships between the muscle mass (resp. benzene concentration) and the remaining covariates not displayed in the paper.

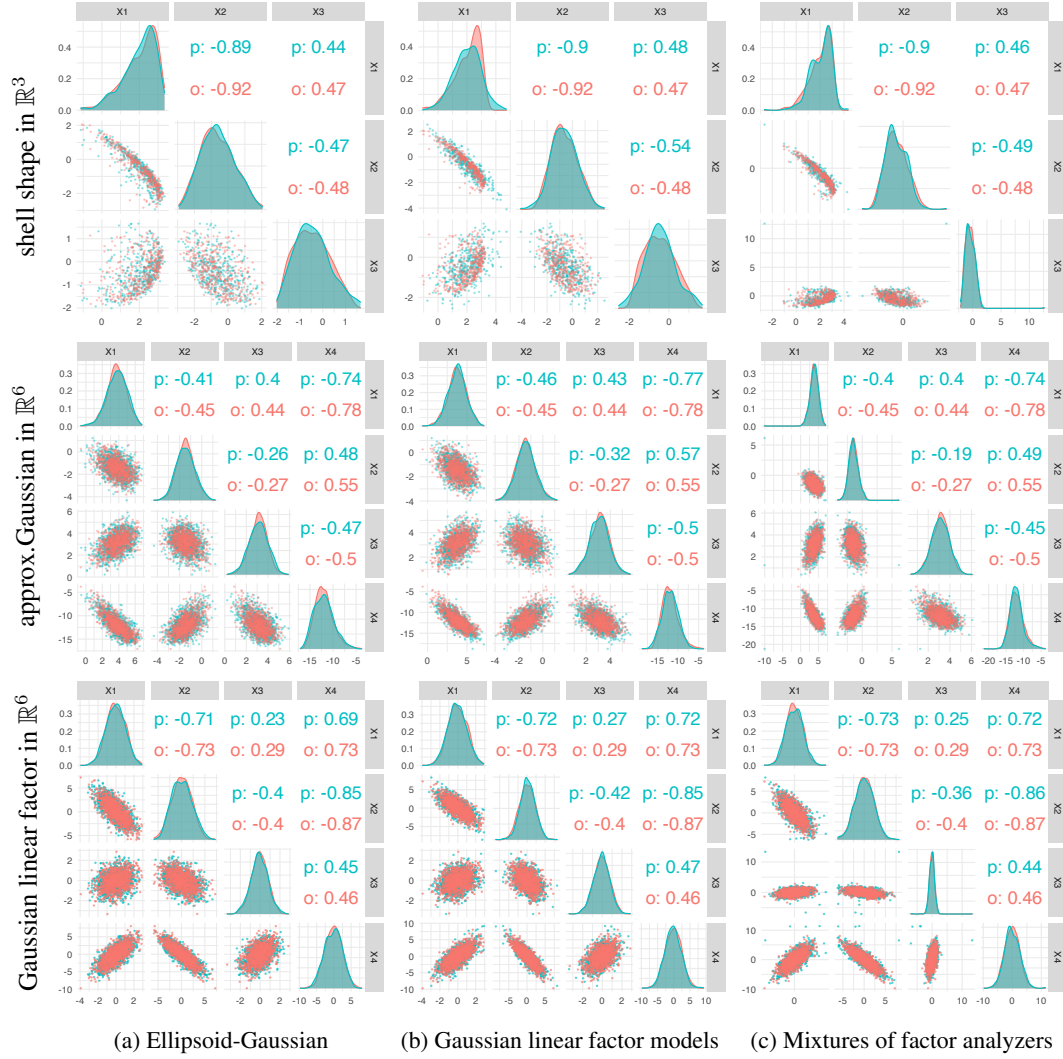


Figure 13: The scatter plot matrices of the posterior predictive (green) juxtaposed with the original data (red) for each method, where the models were fitted to the shell shape in \mathbb{R}^3 with 400 observations (top row), approx. Gaussian data in \mathbb{R}^6 with 1000 observations and 30% random missingness (middle row) and data from Gaussian linear factor model in \mathbb{R}^6 with 1000 observations and 20% random missingness (bottom row). Letters p and o stand for posterior predictive and original data respectively.

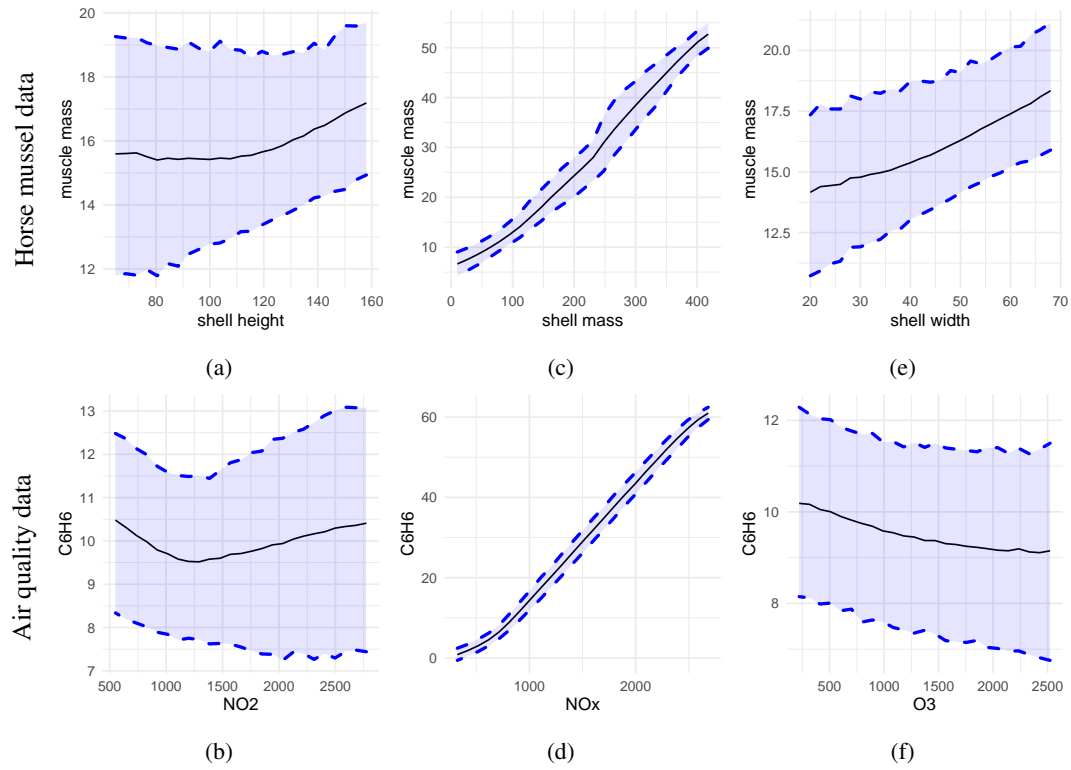


Figure 14: The posterior mean (black) and the 95% credible band (blue ribbon) of muscle mass (top) and the benzene level (bottom) as a function of some covariates while holding other covariates at their sample mean level based on the Ellipsoid-Gaussian fit.

References

- Andrieu, C., & Roberts, G. O. (2009). The pseudo-marginal approach for efficient Monte Carlo computations. *The Annals of Statistics*, 37(2), 697–725.
- Arevalillo, J. M., & Navarro, H. (2015). A note on the direction maximizing skewness in multivariate skew-t vectors. *Statistics & Probability Letters*, 96, 328–332.
- Azzalini, A., & Capitanio, A. (1999). Statistical applications of the multivariate skew normal distribution. *Journal of the Royal Statistical Society: Series B (Statistical Methodology)*, 61(3), 579–602.
- Azzalini, A., & Valle, A. D. (1996). The multivariate skew-normal distribution. *Biometrika*, 83(4), 715–726.
- Azzalini, A., & Capitanio, A. (2003). Distributions generated by perturbation of symmetry with emphasis on a multivariate skew t-distribution. *Journal of the Royal Statistical Society: Series B (Statistical Methodology)*, 65(2), 367–389.
- Banerjee, A., Dhillon, I. S., Ghosh, J., & Sra, S. (2005). Clustering on the unit hypersphere using von Mises-Fisher distributions. *Journal of Machine Learning Research*, 6, 1345–1382.
- Beaumont, M. A. (2003). Estimation of population growth or decline in genetically monitored populations. *Genetics*, 164(3), 1139–1160.
- Bhattacharya, A., & Dunson, D. (2011). Sparse Bayesian infinite factor models. *Biometrika*, 98(2), 291–306.
- Bhattacharya, A., Pati, D., Pillai, N. S., & Dunson, D. B. (2015). Dirichlet–Laplace priors for optimal shrinkage. *Journal of the American Statistical Association*, 110(512), 1479–1490.
- Branco, M. D., & Dey, D. K. (2001). A general class of multivariate skew-elliptical distributions. *Journal of Multivariate Analysis*, 79(1), 99–113.
- Byrne, S., & Girolami, M. (2013). Geodesic Monte Carlo on embedded manifolds. *Scandinavian journal of statistics*, 40(4), 825–845.
- Camden, M. (1989). The data bundle [<https://cran.r-project.org/package=dr>]. *New Zealand Statistical Association*.
- Capitanio, A. (2020). On the canonical form of scale mixtures of skew-normal distributions. *Statistica*, 80(2), 145–160.
- Carvalho, C. M., Chang, J., Lucas, J. E., Nevins, J. R., Wang, Q., & West, M. (2008). High-dimensional sparse factor modeling: Applications in gene expression genomics. *Journal of the American Statistical Association*, 103(484), 1438–1456.
- De Vito, S., Massera, E., Piga, M., Martinotto, L., & Di Francia, G. (2008). On field calibration of an electronic nose for benzene estimation in an urban pollution monitoring scenario [<https://archive.ics.uci.edu/ml/datasets/air+quality>]. *Sensors and Actuators B: Chemical*, 129(2), 750–757.
- Duan, L. L. (2021). Transport Monte Carlo: high-accuracy posterior approximation via random transport [arXiv:1907.10448]. *arXiv Preprint*.
- Einbeck, J., & Dwyer, J. (2011). Using principal curves to analyse traffic patterns on freeways. *Transportmetrica*, 7(3), 229–246.
- Genton, M., & Loperfido, N. (2005). Generalized skew-elliptical distributions and their quadratic forms. *Annals of the Institute of Statistical Mathematics*, 57(2), 389–401.
- Ghahramani, Z., & Hinton, G. E. (1997). *The EM algorithm for mixtures of factor analyzers* (tech. rep. CRG-TR-96-1). Department of Computer Science, University of Toronto.

- Ghosh, J., & Dunson, D. B. (2009). Default prior distributions and efficient posterior computation in Bayesian factor analysis. *Journal of Computational and Graphical Statistics*, 18(2), 306–320.
- Gilbert, P., & Varadhan, R. (2019). *Numderiv: Accurate numerical derivatives* [R package version 2016.8-1.1].
- Gopal, S., & Yang, Y. (2014). Von Mises-Fisher clustering models. *Proceedings of the 31st International Conference on Machine Learning*, 32, 154–162.
- Gupta, A. K. (2003). Multivariate skew t-distribution. *Statistics*, 37(4), 359–363.
- Hoff, P. D. (2009). Simulation of the matrix Bingham–von Mises–Fisher distribution, with applications to multivariate and relational data. *Journal of Computational and Graphical Statistics*, 18(2), 438–456.
- Jupp, P., Regoli, G., & Azzalini, A. (2016). A general setting for symmetric distributions and their relationship to general distributions. *Journal of Multivariate Analysis*, 148, 107–119.
- Kent, J. (1978). Limiting behaviour of the von Mises-Fisher distribution. *Mathematical Proceedings of the Cambridge Philosophical Society*, 84(3), 531–536.
- Kent, J. T., Ganeiber, A. M., & Mardia, K. V. (2013). A new method to simulate the Bingham and related distributions in directional data analysis with applications [arXiv:1310.8110]. *arXiv Preprint*.
- Kim, H.-M. (2008). A note on scale mixtures of skew normal distribution. *Statistics & Probability Letters*, 78(13), 1694–1701.
- Kim, H.-M., & Mallick, B. K. (2003). Moments of random vectors with skew t distribution and their quadratic forms. *Statistics & Probability Letters*, 63(4), 417–423.
- Kingma, D. P., & Welling, M. (2014). Auto-encoding variational Bayes [arXiv:1312.6114]. *arXiv Preprint*.
- Kowal, D. R. (2021). Semiparametric functional factor models with Bayesian rank selection [arXiv:2108.02151]. *arXiv Preprint*.
- Kume, A., & Wood, A. T. A. (2005). Saddlepoint approximations for the Bingham and Fisher-Bingham normalising constants. *Biometrika*, 92(2), 465–476.
- Landsman, Z., Makov, U., & Shushi, T. (2017). Extended generalized skew-elliptical distributions and their moments. *Sankhya A: The Indian Journal of Statistics*, 79(1), 76–100.
- Li, P., & Chen, S. (2016). A review on Gaussian process latent variable models. *CAAI Transactions on Intelligence Technology*, 1(4), 366–376.
- Liu, C., Zhu, J., & Song, Y. (2016). Stochastic gradient geodesic MCMC methods. *Advances in neural information processing systems* 29 (pp. 3009–3017).
- Livingstone, S., & Zanella, G. (2020). The Barker proposal: Combining robustness and efficiency in gradient-based MCMC [arXiv:1908.11812]. *arXiv Preprint*.
- Ma, Y.-A., Chen, T., & Fox, E. (2015). A complete recipe for stochastic gradient MCMC. *Advances in Neural Information Processing Systems*, 28.
- Ma, Z. (2013). Sparse principal component analysis and iterative thresholding. *Annals of Statistics*, 41(2), 772–801.
- McLachlan, G., Peel, D., & Bean, R. (2003). Modelling high-dimensional data by mixtures of factor analyzers. *Computational Statistics & Data Analysis*, 41(3), 379–388.
- Mukhopadhyay, M., Li, D., & Dunson, D. B. (2020). Estimating densities with non-linear support by using Fisher–Gaussian kernels. *Journal of the Royal Statistical Society. Series B (Statistical Methodology)*, 82(5), 1249–1271.

- Murphy, K., Viroli, C., & Gormley, I. C. (2020). Infinite mixtures of infinite factor analysers. *Bayesian Analysis*, 15(3), 937–963.
- Murphy, K., Viroli, C., & Gormley, I. C. (2021). *Imifa: Infinite mixtures of infinite factor analysers and related models* [R package version 2.1.6].
- Pagani, F., Wiegand, M., & Nadarajah, S. (2021). An n-dimensional Rosenbrock distribution for Markov chain Monte Carlo testing. *Scandinavian Journal of Statistics*, online.
- Poworoznek, E. (2020). *Infinitefactor: Bayesian infinite factor models* [R package version 1.0].
- Poworoznek, E., Ferrari, F., & Dunson, D. (2021). Efficiently resolving rotational ambiguity in Bayesian matrix sampling with matching [arXiv:2107.13783]. *arXiv Preprint*.
- Reisinger, J., Waters, A., Silverthorn, B., & Mooney, R. J. (2010). Spherical topic models. *Proceedings of the 27th International Conference on International Conference on Machine Learning*, 903–910.
- Rezende, D. J., Mohamed, S., & Wierstra, D. (2014). Stochastic backpropagation and approximate inference in deep generative models. *Proceedings of the 31st International Conference on International Conference on Machine Learning*, 32, II–1278–II–1286.
- Titsias, M., & Lawrence, N. D. (2010). Bayesian Gaussian process latent variable model. *Proceedings of the 13th International Conference on Artificial Intelligence and Statistics*, 9, 844–851.
- Vihola, M. (2012). Robust adaptive Metropolis algorithm with coerced acceptance rate. *Statistics and Computing*, 22(5), 997–1008.
- Wang, J., & Genton, M. G. (2006). The multivariate skew-slash distribution. *Journal of Statistical Planning and Inference*, 136(1), 209–220.
- Watanabe, S. (2013). A widely applicable Bayesian information criterion. *Journal of Machine Learning Research*, 14(1), 867–897.
- Weisberg, S. (2002). Dimension reduction regression in R. *Journal of Statistical Software*, 7(1), 1–22.
- West, M. (2003). Bayesian factor regression models in the “large p, small n” paradigm. *Bayesian Statistics*, 7, 723–732.
- Wood, A. T. (1988). Some notes on the Fisher–Bingham family on the sphere. *Communications in Statistics - Theory and Methods*, 17(11), 3881–3897.